Acta Geochim (2020) 39(4):539–560
https://doi.org/10.1007/s11631-019-00385-3

ORIGINAL ARTICLE

Comparative geochemical study of the cherty rocks of the Taukha terrane (Sikhote-Alin) and its paleogeodynamic significance

Igor V. Kemkin[1,2] · Raisa A. Kemkina[1,2]

Received: 7 April 2019 / Revised: 5 November 2019 / Accepted: 28 November 2019 / Published online: 4 December 2019

Abstract The article presents the results of a comparative geochemical study of cherts and siliceous–clayey rocks composing the tectono-sedimentary complexes of various structural levels of the Taukha terrain of the Sikhote-Alin Late Jurassic–Early Cretaceous accretionary prism. The data obtained show that the same-aged parts of the cross-sections of the cherty–terrigenous sequences of the terrane lower and middle structural levels are characterized by significantly different contents and distribution patterns of major petrogenic oxides, trace, and rare-earth elements due to their accumulation in various facies of oceanic zones. The set of geochemical data indicates that the formation of both tectono-sedimentary complexes was carried out differently, gradually replacing each others' facies oceanic zones, and started in the near-spreading ridge area, then in the pelagial, and completed in the continental-margin deposition environment. Based on the time interval of the facies conditions changing for each complex (i.e., time of transition from one facies zone to another), the speeds of a paleo-oceanic plate motion (and, correspondingly, the speeds of spreading) for individual intervals of the Jurassic were calculated. Differences in the spreading speeds at various sites of a paleorift zone caused the turning of a paleocontinent margin contour and spreading ridge axis at the perpendicular position, which in turn caused change of the geodynamic mode on the eastern margin of the Paleo-Asian continent at the Jurassic–Cretaceous transition.

Keywords Geochemistry · Radiolarian cherts · Deposition environment · Paleo-Pacific plate · Sikhote-Alin

1 Introduction

The history of formation of folded belts is a chronicle of successive formation of various rock complexes that were formed as a result of combined action of endogenous and exogenous geological processes resulting in different geodynamic settings and leading to formation and growth of new continental crust (Parfenov and Kuzmin 2001; Parfenov et al. 2003; Khanchuk 2006; Buslov 2011; Kröner 2015, etc.) or continental lithosphere (Khanchuk et al. 2016). The study and documentation of rock complexes composing folded belts, as well as their interrelations with each other, allow us to reconstruct a succession of the change of geodynamic modes, and to outline the general regularities and stages of continental crust formation. The Sikhote-Alin orogenic belt is an illustrative example. Based on geological, petro-geochemical, paleobiogeographic, paleomagnetic, structural, and other data, two stages in its formation have been distinguished (c.f., Khanchuk 2000, 2006; Kemkin 2006; Khanchuk et al. 2016)—the Jurassic, corresponding to a geodynamic mode of a convergent subductional margin, and the Early Cretaceous characterized by a transform margin setting along the eastern edge of the Paleo-Asian continent in a combination with subduction margin along its southern tip. The identification of different geodynamic modes is based on documentation of certain structural-material complexes that explicitly indicate their geodynamic affinity. For example,

✉ Igor V. Kemkin
kemkin@fegi.ru

[1] Far East Geological Institute, Far Eastern Branch of Russian Academy of Sciences, Prospect 100-Letiya Vladivostoka, 159, Vladivostok, Russia 690022

[2] Far Eastern Federal University, Soukhanova Street, 8, Vladivostok, Russia 690950

accretionary prisms are indicator complexes for subduction margins. They are intensely deformed and imbricate-thrusted fragments of sedimentary cover of an oceanic plate that are formed at the base of continental or island arc slopes. Transform margins are recognized by thick strata of turbidites characterized by avalanche sedimentation rates and intense shear dislocations.

The change of geodynamic modes on the eastern margin of the Paleo-Asian continent at the Jurassic–Cretaceous transition is associated by most researchers with a change of direction of motion vector of the Paleo-Pacific (Izanagi) plate from north-west to north, which is consistent with data of (Engebretson et al. 1985) calculated on the basis of seafloor magnetic anomalies and hotspots. However, the reasons for change of direction of an oceanic plate motion vector and, correspondingly, the geodynamic modes, are not so obvious and, as a rule, are poorly constrained. This is because reasons have no material characteristics like mineral/chemical composition, structural/textural data or some kind of dislocations and so on. But they determine a set of dominant geological processes that form the structure of individual territories. For example, which material characteristics the difference in spreading rates within different parts of the mid-oceanic ridge possess? But the difference in spreading rates is a cause of the rotation of an oceanic plate in one or another direction, and determines the angle of approach of an oceanic plate to the convergent boundary, thereby determining geodynamic mode in the zone of interaction of two lithospheric plates. However, with no qualitative attributes, causes can be established by the study of quantitative characteristics of other material complexes. Such characteristics are, for example, thickness of the pelagic and hemipelagic parts of the section of the oceanic plate sedimentary cover, the lower the rate of movement, the greater the thickness of accumulated sediments, and vice versa (e.g., Kemkin et al. 2018), the time of crossing of different oceanic facies zones by individual an oceanic plate sites, and the time that individual oceanic plate sites approach the convergent border, etc.

This work presents the results of a comprehensive geochemical study of cherty rocks of the different structural levels of the Taukha terrain of the Sikhote-Alin Late Jurassic–Early Cretaceous accretionary prism. The set of geochemical data together with the lithological and biostratigraphic data for these rocks allowed us to calculate the speeds of the paleo-oceanic plate drifting and identify their differences for individual intervals of the Jurassic time. The difference of spreading speed within the different parts of rift system was, in our opinion, a reason for change of an oceanic plate motion vector and, correspondingly, geodynamic mode on the eastern margin of the Paleo-Asian continent at the Jurassic–Cretaceous transition.

2 Objects of study and their geological position

A comparative geochemical study was carried out for cherty rocks, which make up the Taukha terrain of the Late Albian–Early Cenomanian Sikhote-Alin orogen, and document information about their oceanic origin and the history of an oceanic plate drift, within which they were accumulated. The Taukha terrane represents a fragment of the Late Jurassic–Early Cretaceous accretionary prism, which was formed as a result of successive accretion of different-aged and different-facies formations of the Paleo-Pacific (fragments of paleoguyots and sedimentary cover of abyssal plain) to the south-eastern margin of the Paleo-Asian continent during subduction of an oceanic lithosphere (Khanchuk 2006; Kemkin 2006; Khanchuk et al. 2016, etc.). The Taukha terrane composes the south-eastern part of the Sikhote-Alin orogenic belt. The Taukha terrane is unconformable overlapped by Late Cretaceous volcanic and volcano-sedimentary rocks, and crops out only in isolated erosion "windows" (Fig. 1). The structure of the terrane is characterized as a package of multiple alternation of tectonic slices (Fig. 2) composed of different-aged and intensively deformed fragments of an oceanic plate sedimentary cover, otherwise called Oceanic Plate Stratigraphy Sequence (Berger and Winterer 1974; Isozaki et al. 1990, etc.). Based on the lithological-biostratigraphic and structural data, 3 different-aged tectono-sedimentary complexes (Erdagou, Gorbousha and Skalistorechka) are distinguished within the terrain (Kemkin and Kemkina 1998, 2000; Kemkin 2006), which represent its different structural levels and reflect the succession of subduction and partial accretion of the Palae-Pacific oceanic plate.

The Erdagou Complex (lower unit) is composed of tholeiitic basalts and, overlaying them, cherts and clayey cherts of late Jurassic–Early Berriasian (also referred as the Erdagou Suite). The clayey cherts gradually transition into the Early-Middle Berriasian siliceous mudstones, and then into the Late Berriasian-Valanginian terrigenous rocks (mudstones, siltstones, and sandstones—so-called the Silinka Suite), which, in turn, are overlain by the Valanginian-Barremian chaotic formations (subduction mélange). The thickness of basalts and cherts is slightly more than 150 m, and the thickness of terrigenous rocks within the tectonic slices is 350–700 m. The thickness of the chaotic horizons in different areas varies from 100–200 to 400 m. A typical cross-section of the Erdagou Complex has been studied on the right bank of the Benevka River and is presented in Fig. 3.

The Gorbusha Complex (middle unit) consists of the Middle-Late Triassic limestones up to 500 m thick (Tetyukha Suite) with high-titanium alkaline basalts at the bottom that are interpreted as fragments of paleoguyots and

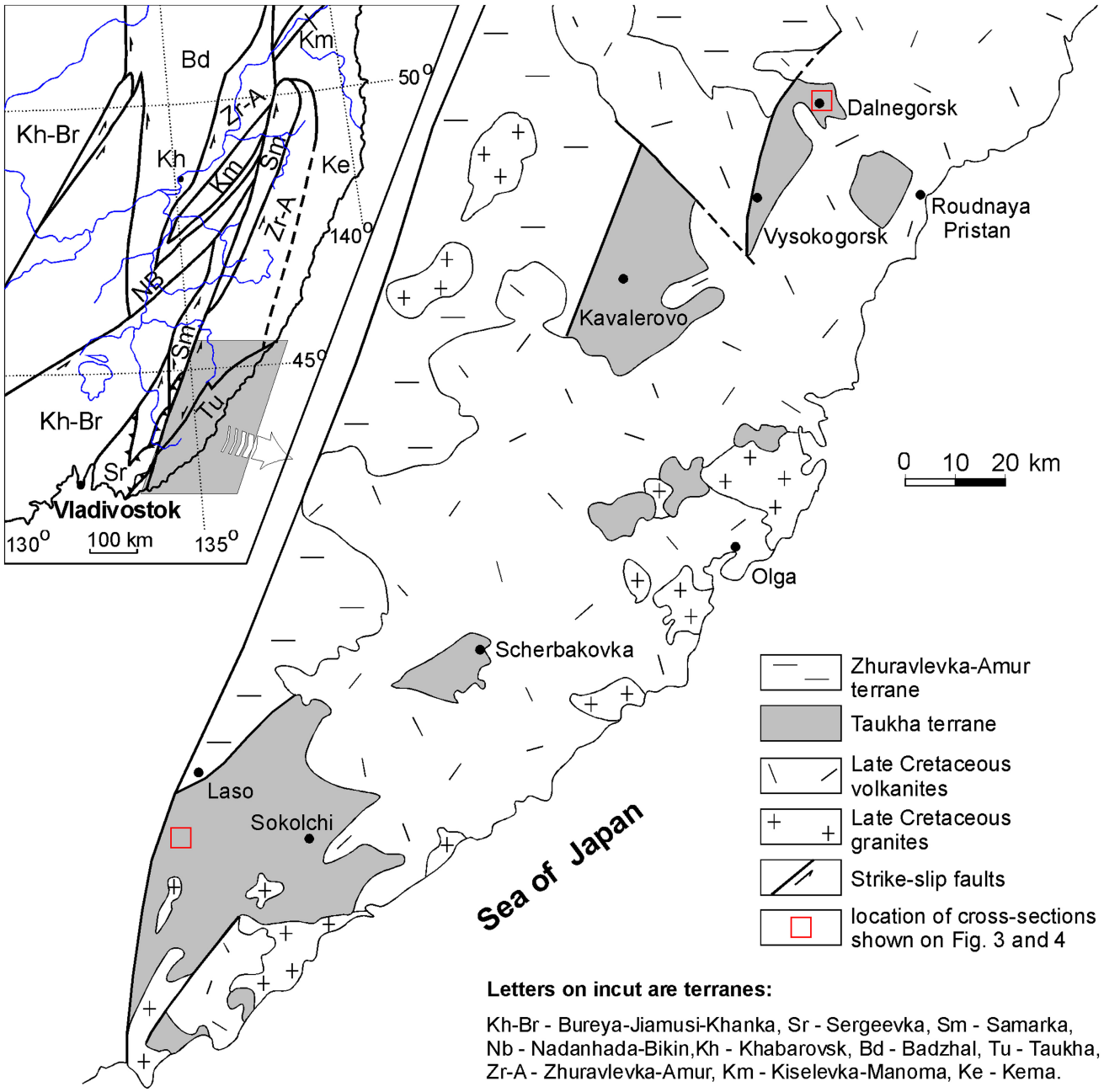

Fig. 1 Tectonic scheme of the Southern Sikhote-Alin south-eastern part (after Kemkin and Kemkina 2000 with additions)

fourfold repeating chert-terrigenous sequence (Gorbusha Suite) overlaying them. Each sequence is composed of the Early Triassic-Late Jurassic cherts and clayey cherts (~ 100 m thick), which are gradually replaced, further up, by the Middle Kimmeridgian–Middle Tithonian siliceous mudstones, and then late Late Tithonian–Berriasian mudstones, siltstones, and sandstones. Terrigenous rocks are overlapped by Berriasian-Valanginian chaotic formations. The thickness of terrigenous rocks in various areas is 300–500, less often 750 m. The thickness of subduction mélange formations is 100–400 m. A typical cross-section of the Gorbusha Complex is exposed on the left bank of the Roudnaya River in the Dalnegorsk Town and is presented in Fig. 4.

The Skalistorechka Complex (upper unit) is studied in less detail because it is of limited extent with small and scattered outcrops. Therefore, the interrelation between most lithological varieties of rocks has not been studied enough. This complex is made up of Late Devonian–Early Permian limestones (about 400 m) associated with high-titanium alkaline basalts (Skalistorechka Suite) that also are interpreted as fragments of paleoguyots and cherts,

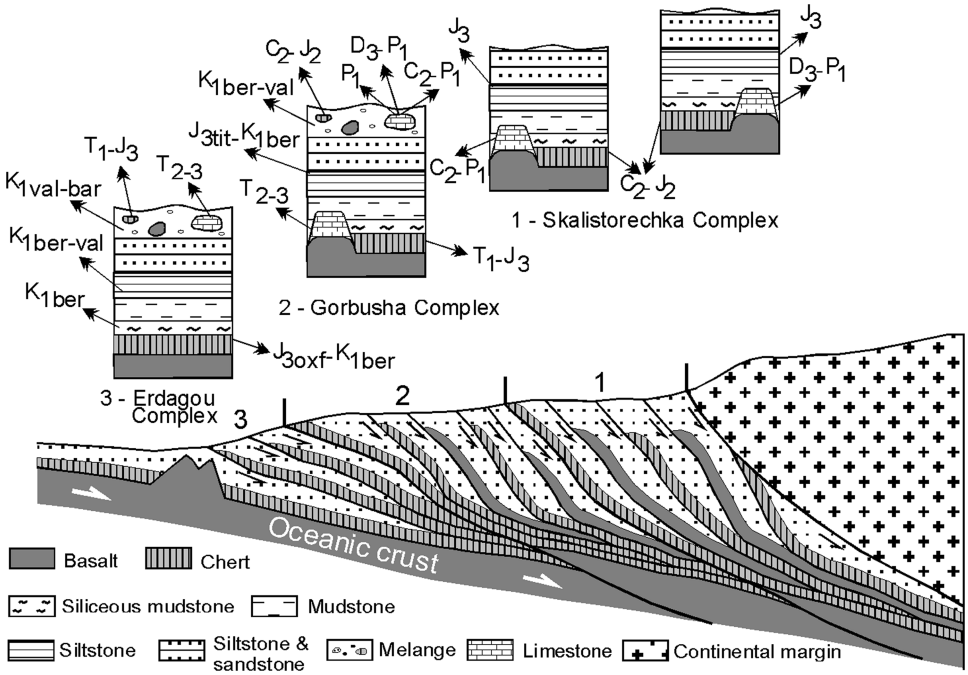

Fig. 2 Reconstructed structure of the Sikhote-Alin Taukha terrain, before orogenic deformations (after Kemkin et al. 2016 with additions)

clayey cherts, and terrigenous rocks (Pantovaya Suite). The age of cherty rocks varies from Carboniferous to Middle Jurassic according to the data obtained from separate outcrops. The terrigenous rocks associated with cherty rocks are Late Jurassic in age. The true thickness of cherts and terrigenous rocks has not been established due to their scattered outcrops.

3 Methods

To find out geochemical features of different-aged parts (i.e., different stratigraphic levels) of the Taukha terrane chert-terrigenous sequences, samples of cherts and siliceous mudstones, from which radiolarian fossils were previously extracted and age determined, were selected in the present study. At first, all rock samples were crushed into pieces up to 1 cm in size. Each piece was viewed under the binocular and the freshest of them (without altered surfaces and any veinlets) were selected for further grinding and powdering. All powdered samples were given to the Analytic Center of the Far East Geological Institute (Russia), where they were examined. Major element abundances were measured by ICP AES method using iCAP 6500Duo spectrometer, and SiO_2 and H_2O by the conventional wet chemical method. Trace elements and REEs contents were analyzed by ICP MS method using Agilent 7500C spectrometer. The detailed procedures of ICP MS and ICP AES analysis are given in (Barcelo 2003). The precision of the analyses was generally 2%–5% for major oxides and 5%–10% for REE and trace elements.

For calculating value of Ce anomaly we used the NASC (North America Shale Composite)-normalized ratio Ce/Ce*(1) = $(Ce_{samp}/Ce_{NASC})/0.5((La_{samp}/La_{NASC}) + (Pr_{samp}/Pr_{NASC}))$, according to (Murray 1994; Murray et al. 1990, 1991) and Ce/Ce*(2) = $(Ce_{samp}/Ce_{NASC})/(2*Pr_{samp}/Pr_{NASC} - Nd_{samp}/Nd_{NASC})$, according to (Lawrence and Kamber 2006; Lawrence et al. 2006; Alexander et al. 2008). The REE contents of NASC are from (Gromet et al. 1984). In view of the anomalous behavior of La, Lu, and Ce in the seawater, some geochemical parameters using these elements were quantified in several ways. The ratios of LREE relatively HREE were determined by the following equations: $(Lu/La)_n = (Lu_{samp}/Lu_{NASC})/(La_{samp}/La_{NASC})$, $(Pr/Er)_n = (Pr_{samp}/Pr_{NASC})/(Er_{samp}/Er_{NASC})$, and $(Pr/Yb)_n = (Pr_{samp}/Pr_{NASC})/(Yb_{samp}/Yb_{NASC})$. The ratios of La/Ce were calculated using following formulas: $(La/Ce)_n = (La_{samp}/La_{NASC})/(Ce_{samp}/Ce_{NASC})$ and $(La^*/Ce^*)_n = (3*Pr_{samp}/Pr_{NASC} - 2*Nd_{samp}/Nd_{NASC})/(2*Pr_{samp}/Pr_{NASC} - Nd_{samp}/Nd_{NASC})$.

4 Analytical results

To reconstruct the history of sedimentation on an oceanic plate and to fix the moments of passage of individual sites of an oceanic plate through different facies oceanic zones, it is necessary to have the fairly complete and well-dated fragments of the primary section of its sedimentary cover. In the Taukha terrane, the fragments with preserved primary gradual lithological transitions from cherts to terrigenous rocks have been studied within the Gorbusha and

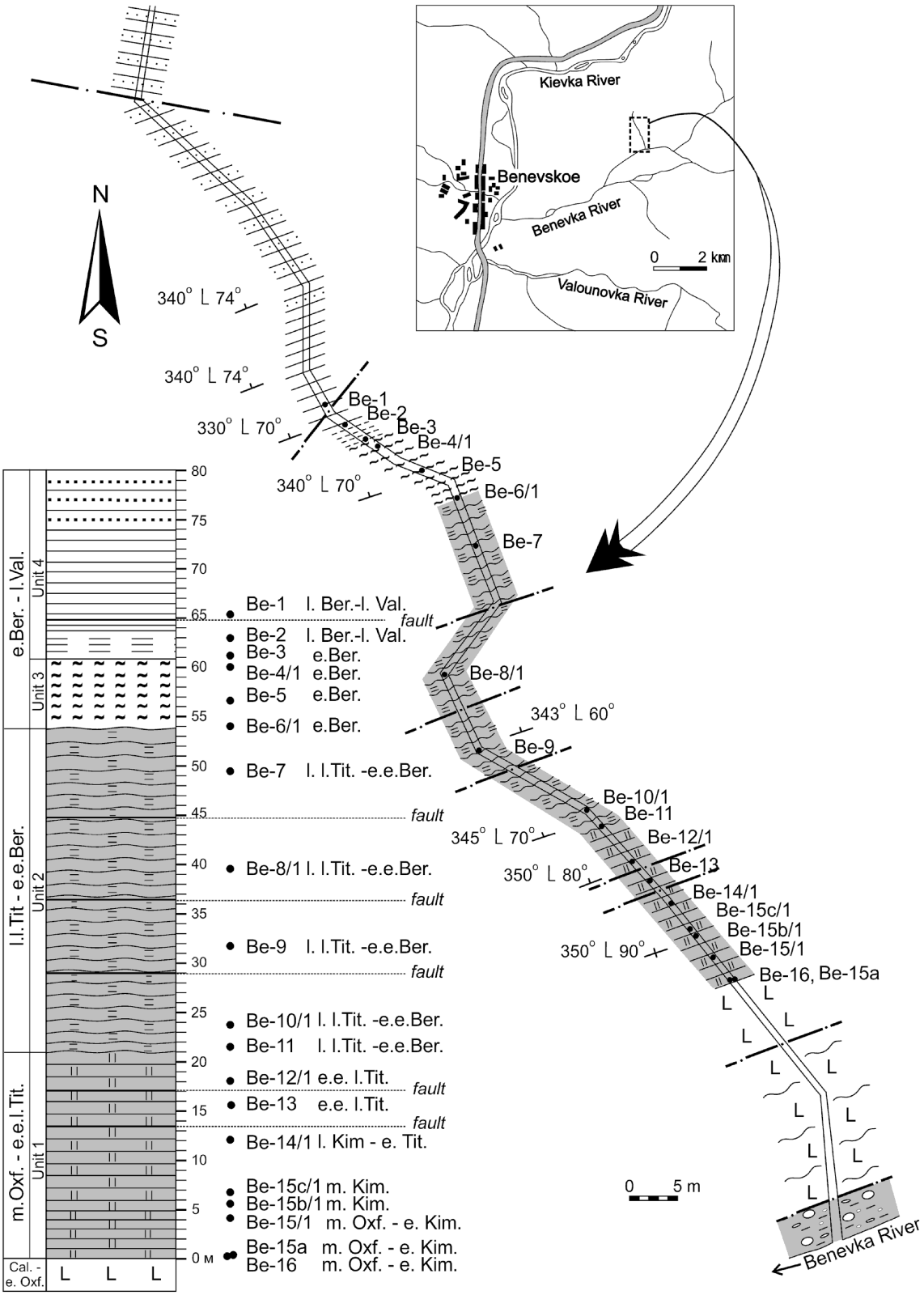

Fig. 3 Structure of the Erdagou Complex on the right bank of the Benevra River (after Kemkin and Taketani 2008 with additions). See legend on Fig. 4

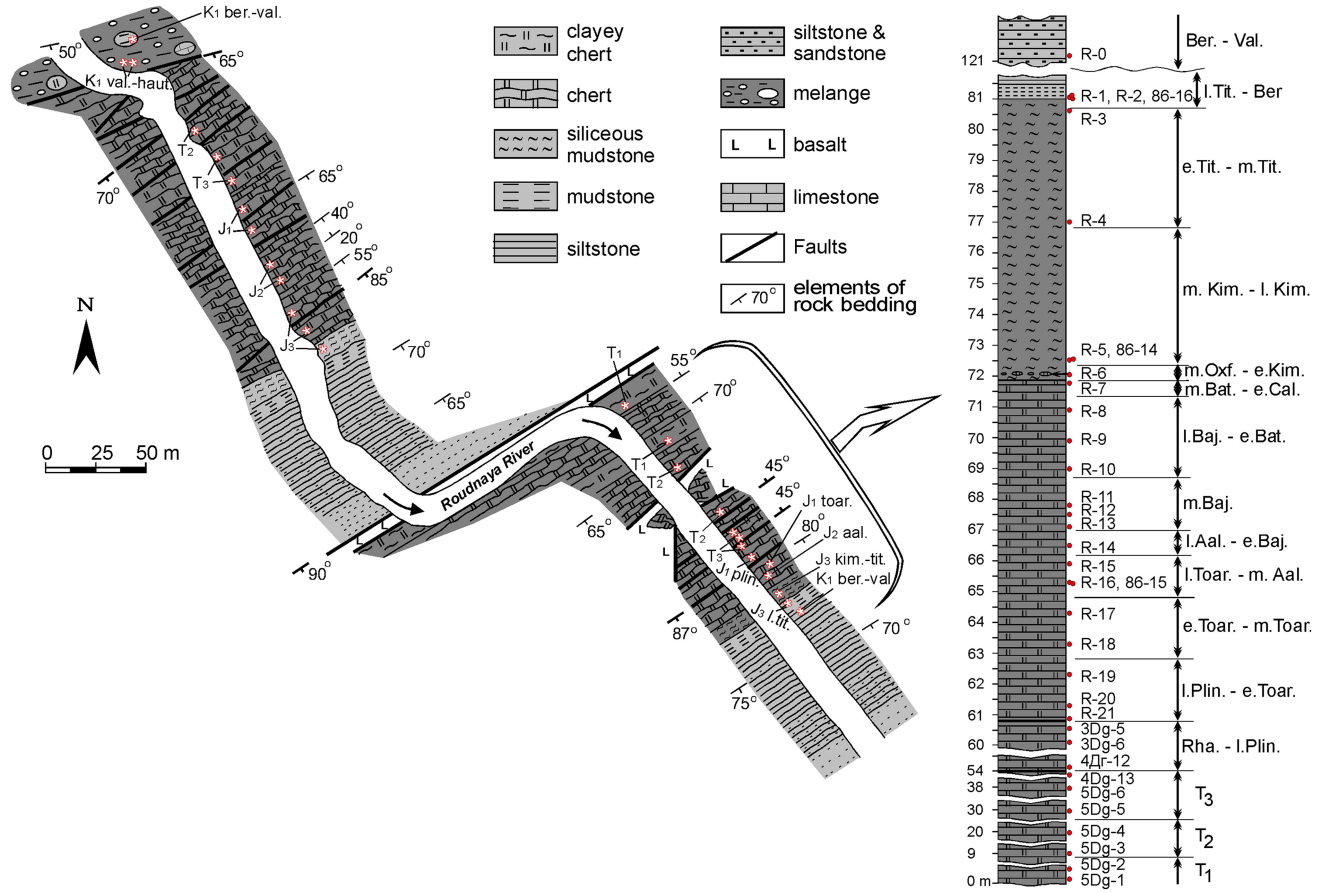

Fig. 4 Structure of the Gorbusha Complex in the Dalnegorsk Town, riverbanks outcrops (after Kemkin and Kemkina 2000 with additions)

Erdagou Complexes (Figs. 3, 4). The geochemical characteristics of the cherty rocks of these complexes are presented in Tables 1, 2, 3, 4 and 5 in "Appendix" section.

4.1 Major element composition

The dominant component in the cherts and siliceous–clayey rocks, which is quite natural, is silicon dioxide (SiO_2), the content of which gradually decreases from 92.76 and 83.10 wt% in cherts up to 77.90 and 66.73 wt% in siliceous mudstones (hereinafter, the first values correspond to the Gorbusha Complex, and the second—to Erdagou one).

The relatively low SiO_2 contents in siliceous mudstones are caused by their accumulation in the peripheral parts of an ocean, where significant amounts of terrigenous suspension are delivered (these rocks consist of 60% or more of clayey terrigenous minerals, 10%–15% aleuritic particles and up to 25% radiolarian shells). Some variations of SiO_2 contents (from 92.76–85.64 to 83.10–76.20 wt%) are also noted for cherts of the bottom part of the studied sections. However, this fluctuation of SiO_2 can probably be explained by the fact that the stratigraphically lowermost cherts were accumulated in the immediate vicinity from the spreading ridge, where periodic amplification of hydrothermal activity produced more metalliferous solutions, which supplied chert sediments with a large amount of Fe and Mn oxyhydroxides. This assumption is fully consistent with the data on the distribution of such oxides as Al_2O_3 and Fe_2O_3, the concentrations of which vary in diametrically opposite directions. From the bottom layers of chert-terrigenous sequences of both Complexes to the upper sections, Fe_2O_3 content gradually decreases from 8.54 and 13.41 wt% in cherts to 2.43 and 6.86 wt% in siliceous mudstones. On the contrary, Al_2O_3 content gradually increases from 1.00 and 3.32 to 11.12, and 14.90 wt% in the direction from cherts to siliceous mudstones (Tables 1, 2 in "Appendix" section).

Geochemical data show that TiO_2 and MnO contents in the Taukha terrane cherty rocks are much less than the contents of Al_2O_3 and Fe_2O_3, however the stratigraphic variations of their distribution are analogous to the above two oxides. Their MnO content shows a complete mirror image of TiO_2. From bottom to up the sections of both chert-terrigenous sequences MnO content gradually decreases from 0.26 and 3.21 to 0.08 and 0.09 wt%. By

contrast, content of TiO_2 increases from 0.03 and 0.11 wt% (in cherts) to 0.41 and 0.62 wt% (in siliceous mudstones). In addition, it should be noted that siliceous mudstones in both sequences are characterized by slightly higher contents of K_2O, MgO and Na_2O relative to cherts (Tables 1, 2 in "Appendix" section) that, apparently, is due to the presence of clay minerals in them.

According to the data of a number of researchers studying see-bottom sediments and sedimentary rocks (e.g., Bonatti et al. 1971; Brueckner and Snyder 1985; Taylor and McLennan 1985; Hein and Koski 1987; Brueckner et al. 1987; Murray 1994; Dubinin 1994, 1998; Zhang et al. 2006, etc.), some chemical elements are immobile during post-sedimentation processes (diagenesis, hypergenesis, and metamorphism). Such geochemical behavior of individual elements in marine sediments is used by sedimentologists for the reconstruction of depositional environments (e.g., Murray et al. 1991; Murray 1994; Halamič et al. 2001; Li 2000; Chen et al. 2006; Kang et al. 2011; Thassanapak et al. 2011, etc.). By the researches of the above-mentioned authors, it is established that high contents of such elements as Al, Ti, K, Na, and some others in the sea-bottom sediments are caused by presence of terrigenous material that is characteristic of the continental-margin depositional environment. On the contrary, in the vicinity of spreading ridges, which produce not only basaltic lava but also metalliferous hydrothermal solutions, the sea-floor sediments are enriched in such elements as Fe, Mn, Co, Ni, Zn, V, Pb, Y, and some others.

Analysis of the accumulated data on distribution of chemical elements in the sea-floor sediments of various facies oceanic zones made it possible to develop a number of petrochemical modules and discriminatory diagrams using them, in which the fields of the continental-margin, pelagic and near-spreading ridge sedimentation zones are clearly separated (e.g., Murray 1994; Kunimaru et al. 1998; Strekopytov et al. 1999; Halamič et al. 2001; Kato et al. 2002; Zhang et al. 2006; Chen et al. 2006; Du et al. 2007; Thassanapak et al. 2011, etc.). Among numerous petrochemical modules the $Al_2O_3/(Al_2O_3 + Fe_2O_3)$, MnO/TiO_2, Fe_2O_3/TiO_2, $Fe_2O_3/(100\text{-}SiO_2)$, $Al_2O_3/(100\text{-}SiO_2)$ are considered to be most informative for discriminating marine depositional environments. According to the abovementioned researchers, the $Al_2O_3/(Al_2O_3 + Fe_2O_3)$ value less than 0.35 characterizes the near-spreading ridge depositional zone (within a distance of 400 km), whereas 0.35–0.70 indicates the pelagic (open-ocean) environment, and 0.55–0.90 corresponds to the continental-margin one. The calculated $Al_2O_3/(Al_2O_3 + Fe_2O_3)$ values for cherts and clayey cherts of both the Gorbusha and Erdagou Complexes show that accumulation of these sediments took place partly in the near-spreading zone, and mainly within the pelagial, whereas the siliceous mudstones were accumulated in the near continental-margin facies zone (Fig. 5a). It should be noted that the near-spreading ridge depositional environment is discriminated only for the lowermost layers of cherts of both chert-terrigenous sequences that are caused by high Fe_2O_3 contents in them (Tables 1, 2 in "Appendix" section). As mentioned above, the sea-floor sediments in the vicinity of spreading ridge are subjected to strong influence of metalliferous hydrothermal solutions, which can extended to several hundred kilometers. For the same reason (i.e., high contents of Fe_2O_3), the similar pattern is also noted in the Fe_2O_3/TiO_2 versus $Al_2O_3/(Al_2O_3 + Fe_2O_3)$ and $Fe_2O_3/(100\text{-}SiO_2)$ versus $Al_2O_3/(100\text{-}SiO_2)$ diagrams, where figurative points of cherts from lowermost parts of both sequences are located in the near-spreading area (Fig. 5c, d).

According to (Sugisaki et al. 1982; Kunimaru et al. 1998; Kang et al. 2011, etc.), the value of MnO/TiO_2 ratio is also a distinct indicator of belonging to concrete facies oceanic zones. For example, the value of this ratio in the sea-floor sediments < 0.5 characterizes the continental-margin environment, whereas > 0.5 characterizes the pelagial. In Fig. 5b it can be seen that the figurative points of cherts and clayey cherts of the Gorbusha and Erdagou Complexes are located mainly in the field of pelagic sedimentation zone, whereas samples of siliceous mudstones and one sample of clayey chert fell in the field of the near continental-margin sedimentation zone.

4.2 Trace element composition

In comparison with the averaged terrigenous rock (e.g., PAAS—Post Archean Average Shale), the contents of trace elements, supplied to seafloor sediments as terrigenous particles, in cherty rocks of the Gorbusha and Erdagou Complexes are significantly lower (Tables 2, 3 in "Appendix" section), that explicitly indicates that above mentioned cherty rocks accumulated out of zone continental-margin sedimentation. This is visually illustrated by such elements as Zr, Rb, Hf, and Th, the contents of which are respectively 5–45, 1.5–37, 4.5–45, and 2.3–22.5 times lower than those in PAAS (Taylor and McLennan 1985). In siliceous mudstones, the concentrations of these elements are higher, but also less than in PAAS respectively 1.5–2, 1.4–1.5, 1.1–1.2 and 1.2–1.4 times. On the contrary, the contents, for example, Pb, Cu, Ni, Fe, and Mn, which are mainly supplied into sediments with metalliferous hydrothermal solutions, are rather higher than those at PAAS in 1.2–3 times and even more for individual samples. It should be also noted that the contents of elements mentioned above gradually change (increase or decrease) up the section of both complexes (i.e., from cherts to siliceous mudstones). In the Tables 2 and 3 in "Appendix"

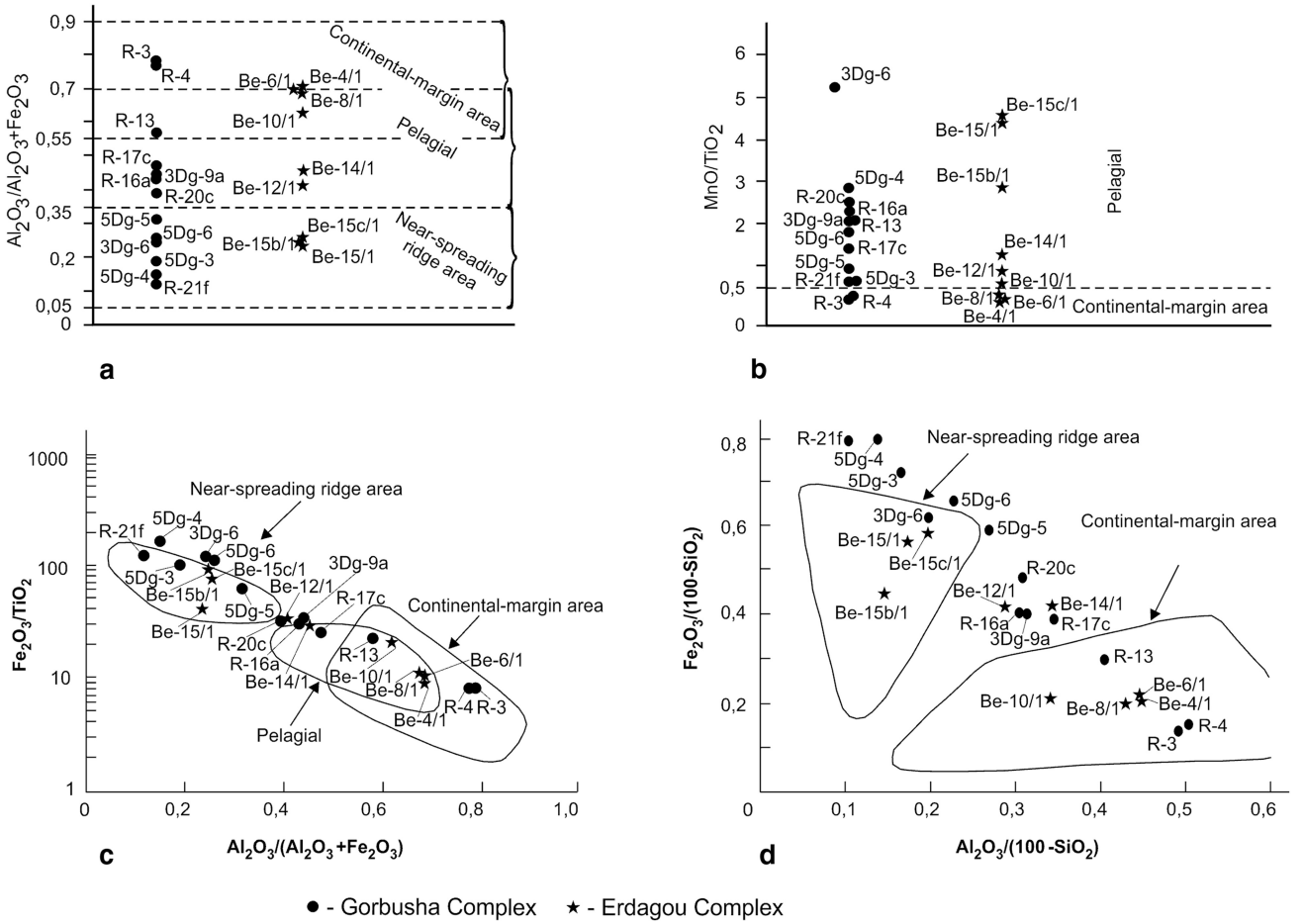

Fig. 5 Diagrams of ratios of petrogenic oxides (according to Murray 1994) and position on them the figurative points of the Erdagou and Gorbusha Complexes cherty rocks

section it can be seen that contents, for example, of Zr and Rb, the values of which are determined by amount of terrigenous material, increase respectively from 4.69 ppm and 8.19 ppm (Gorbusha cherts) and 5.16 and 11.76 ppm (Erdagou cherts) to 31.31 ppm and 134.74 ppm (Gorbusha siliceous mudstones) and 166.88 ppm and 112.29 ppm (Erdagou siliceous mudstones). This indicates that cherts accumulated more in the pelagic environment than the siliceous mudstones. By contrast, the contents of Cu and Ni supplied with metalliferous hydrothermal solutions gradually decrease respectively from 71.39 and 53.24 ppm (Gorbusha cherts) and 178.19 ppm and 168.04 ppm (Erdagou cherts) to 20.09 ppm and 20.04 ppm (Gorbusha siliceous mudstones) and 50.34 ppm and 53.39 ppm (Erdagou siliceous mudstones). This allows us to conclude that siliceous mudstones accumulated at a much greater distance from the spreading ridge than cherts.

The Ti/V and V/Y ratios, that are widely used for reconstruction of depositional environments, also agree with the above conclusion. The values of Ti/V $\geq$ 40, and V/Y $\leq$ 2 characterize the continental-margin facies zone, while for the near-spreading ridge zone, the values of these ratios are Ti/V $\leq$ 7 and V/Y $\geq$ 2 (Murray et al. 1991; Li 2000; Kang et al. 2011). For the pelagic zone, the value of Ti/V ratio is in range of 7–40, and the value of V/Y coincides with that of near-spreading ridge zone. Geochemical data of the Taukha terrane cherty rocks show that the values of their Ti/V and V/Y ratios correspond mainly to the pelagic sedimentation area (Fig. 6a, b). Two samples, however, fell in the transition zone between continental-margin sedimentation area and pelagic sedimentation area due to slightly high content of Y in one clayey chert and Ti in one siliceous mudstone.

4.3 Rare earth element composition

Many geochemical studies have shown that REEs are generally unaffected by diagenetic, hypergenic, and metamorphic fractionation and alteration and, are therefore, practically immobile during post-sedimentation processes, that allow their use for discrimination of the depositional environments of marine sedimentary rocks formation

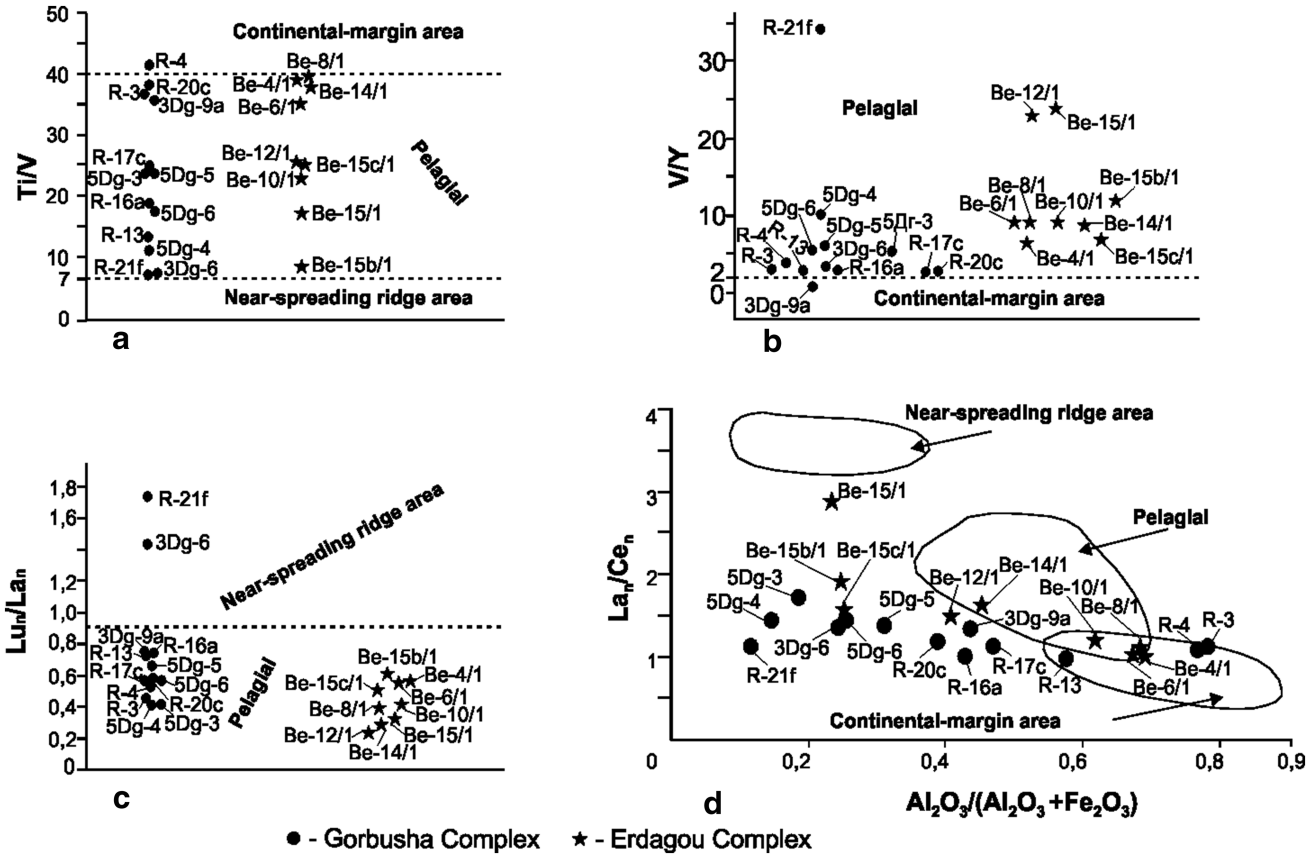

Fig. 6 Diagrams of ratios Ti/V, V/Y, Lu_n/La_n and La_n/Ce_n (according to Murray et al. 1991; Murray 1994) and position on them the figurative points of the Erdagou and Gorbusha Complexes cherty rocks

(Ruhlin and Owen 1986; Murray et al. 1990, 1991; Murray 1994; Dubinin 1994, 1998; Kato et al. 2002; Chen et al. 2006). It is known that the supplying marine sea-floor sediments with REE are brought about first of all by the adsorption of these elements from seawater, and additionally by the settling of terrigenous and ore mineral particles and their incorporation into the sediments in the sedimentation zone on the continental margins. Hence, the total REE concentration in the marine sediments, ultimately, is determined by duration of interaction of sediments with seawater and the amount of terrigenous material. In this connection, the total REE concentrations are informative mainly for estimating the rate of sedimentation, while the individual elements of this group, due to their chemical properties, reveal certain regularities in their distribution depending on the specific environmental conditions.

One of the informative indicators of facies environments of oceanic sedimentation is the content of Ce expressed by the value of the cerium anomaly (Ce/Ce*). This parameter, according to (Courtois and Hoffert 1977; Shimizu and Masuda 1977; Yamamoto 1987; Sholkovitze 1990; Toyoda et al. 1990; Murray et al. 1990, 1991; Murray 1994; Strekopytov et al. 1999), is significantly different for different oceanic facies zones. In the continental-margin depositional area the Ce/Ce* value ranges from 0.9 to 1.3, in the pelagic depositional area the Ce anomalies ranging from 0.23 to 0.96, and in the near-spreading depositional area (in a distance of 400 km from spreading ridge) the Ce/Ce* value is 0.03–0.36. The significant cerium decreasing from continental-margin depositional area to the near-spreading depositional area is explained by the oxidation of this element in trivalent form in oxygen-rich waters of the central part of an ocean to its poor solubility in tetravalent form and precipitation from the waters column. Extremely lower Ce content within the near-spreading ridge depositional zones is caused by addition sorption of this element by Fe and Mn oxyhydroxides, which enter the seawater in large amounts with metalliferous hydrothermal solutions.

The Ce anomaly values in cherts of the Gorbusha and Erdagou Complexes are ranged within 0.698–0.983 and 0.34–0.94, respectively (Tables 4, 5 in "Appendix" section), indicating that these rocks have accumulated within pelagic depositional environment, and for the four first meters of the Erdagou Complex chert section this is a zone immediately adjacent to the spreading ridge. The Ce/Ce*

ratio in siliceous mudstones is 0.981–0.983 (Gorbusha Complex) and 0.91–0.92 (Erdagou Complex), which indicates the peripheral zone of an ocean adjacent to the continental-margin depositional area. Analysis of the Ce/Ce* values in cherty rocks of both complexes shows gradually increasing of this parameter up the cross-sections that evidenced motion of the sites of an oceanic floor, where cherty rocks were accumulated, towards the continent.

It should be noted that Lawrence and Kamber (2006) referring to the anomalous behavior of some REEs (La, Ce, Gd, Lu, and some others) suggested calculating Ce anomaly avoiding La but using Pr and Nd. The calculated Ce anomaly values [$Ce/Ce^* = (Ce_{samp}/Ce_{NASC})/(Pr_{samp}/Pr_{NASC} + (Pr_{samp}/Pr_{NASC} - Nd_{samp}/Nd_{NASC}))$] are very slightly different from those defined in the first way (see Tables 4, 5 in "Appendix" section) and display analogous distribution trend, gradually increasing from the lowermost chert layers up the sections to the siliceous mudstones.

Geochemical studies show that light REEs are more actively absorbed by the suspended particles and Fe and Mn oxyhydroxides in seawater (Piper and Graef 1974; Elderfield and Greaves 1982; German et al. 1990; Murray et al. 1991; Sholkovitz et al. 1994; Kato et al. 1998; Dubinin 2006, etc.). As a result, the LREE/HREE ratio in sea-floor sediments successively decreases from continental marginal sedimentation environments to pelagic ones. NASC-normalized La/Yb and Lu/La ratios are usually used to determine enrichment of heavy REE relatively light REE. Murray et al. (1991) reported that in the near-spreading ridge depositional zone the Lu_n/La_n value ranging from 1.55 to 0.87, and within the pelagic sedimentation area it decreasing to 0.37 and even somewhat less. The geochemical data of cherts and siliceous mudstones of both tectonostratigraphic units of the Taukha terrane show that as a whole the values of their Lu_n/La_n ratios correspond to pelagic depositional environment (Fig. 6c). For most cherty rocks Lu_n/La_n ratio ranges from 0.41 to 0.75 for Gorbusha Complex and from 0.24 to 0.61 for Erdagou Complex (Tables 4, 5 in "Appendix" section). Two samples of the Gorbusha Complex cherts, however, exhibit rather high HREE enrichment. The values of their Lu_n/La_n ratio are 1.74 and 1.43, corresponding to the near-spreading ridge depositional environment. The greater LREE depletion of these chert samples is probably related to high Fe_2O_3 content (Table 1 in "Appendix" section) that in turn, might be attributed to the stronger periodical impact of metalliferous fluids during their accumulation. Moreover, the cherts and siliceous mudstones of the Taukha terrane display no regularity of LREE/HREE ratio (Tables 4, 5 in "Appendix" section) based upon calculation of the enrichment of HREE relatively LREE using the NASC-normalized ratios of Pr_n/Er_n and Pr_n/Yb_n. (Lawrence and Kamber 2006; Lawrence et al. 2006; Alexander et al. 2008).

The La_n/Ce_n versus $Al_2O_3/(Al_2O_3 + Fe_2O_3)$ discrimination diagram developed by Murray (1994) for the chert-terrigenous Franciscan Complex is considered to be informative for the reconstruction of different oceanic facies zones. On this diagram, the points of cherty rocks of both tectono-sedimentary complexes of the Taukha terrane are placed successively (i.e., stratigraphically) from the field of the near-spreading depositional zone through the field of the pelagic depositional area to the field of continental-margin sedimentation. However, due to somewhat low content of La in the cherts of the lowermost parts of Gorbusha and Erdagou sections, their data points lay a little below the facies fields of cherts of the Franciscan Complex (Fig. 6d).

As Alexander et al. (2008) showed, the ratios of contents of some REEs in sea-bottom sediments can be used for quantifying the extent of conservative mixing of high-T hydrothermal fluid with seawater, and, correspondingly, for assessing the contribution of the hydrothermal fluid input on the distribution pattern of REEs in these sediments. These authors developed a number of diagrams (Y/Ho vs. Eu/Sm, Y/Ho vs. Sm/Yb and Sm/Yb vs. Eu/Sm), in which the areas with different proportions of mixing of the seawater and hydrothermal fluid are denoted. On these diagrams the points of the Taukha terrane cherty rocks grouped close to the area of the hydrogenetic Fe–Mn crusts and rather far from the area of seawater unaffected by hydrothermal fluid (Fig. 7). This indicates that seawater surrounding cherty sediments during their accumulation was enriched in Fe–Mn colloidal particles, which precipitated together with biogenic silica and incorporated to the sea-bottom deposits. The direct evidence of this is the value of Y/Ho ratio, which is significantly lower in the studied cherty rocks (15.60–32.92, Tables 4, 5 in "Appendix" section) than that of seawater (40–90). It is known that Ho is more sorbable than Y and is scavenged by the surficial layer of Fe–Mn colloidal particles more actively (e.g., Bau and Dulski 1996). The low value of Y/Ho ratio in the studied cherty rocks suggest that process of chert-accumulation can be accompanied with impact of metalliferous hydrothermal solutions. It should be noted that more intensive impact of this solution is observed in the lowermost chert layers that may be explained by their accumulation in the sedimentation zone located closely to the near-spreading ridge area.

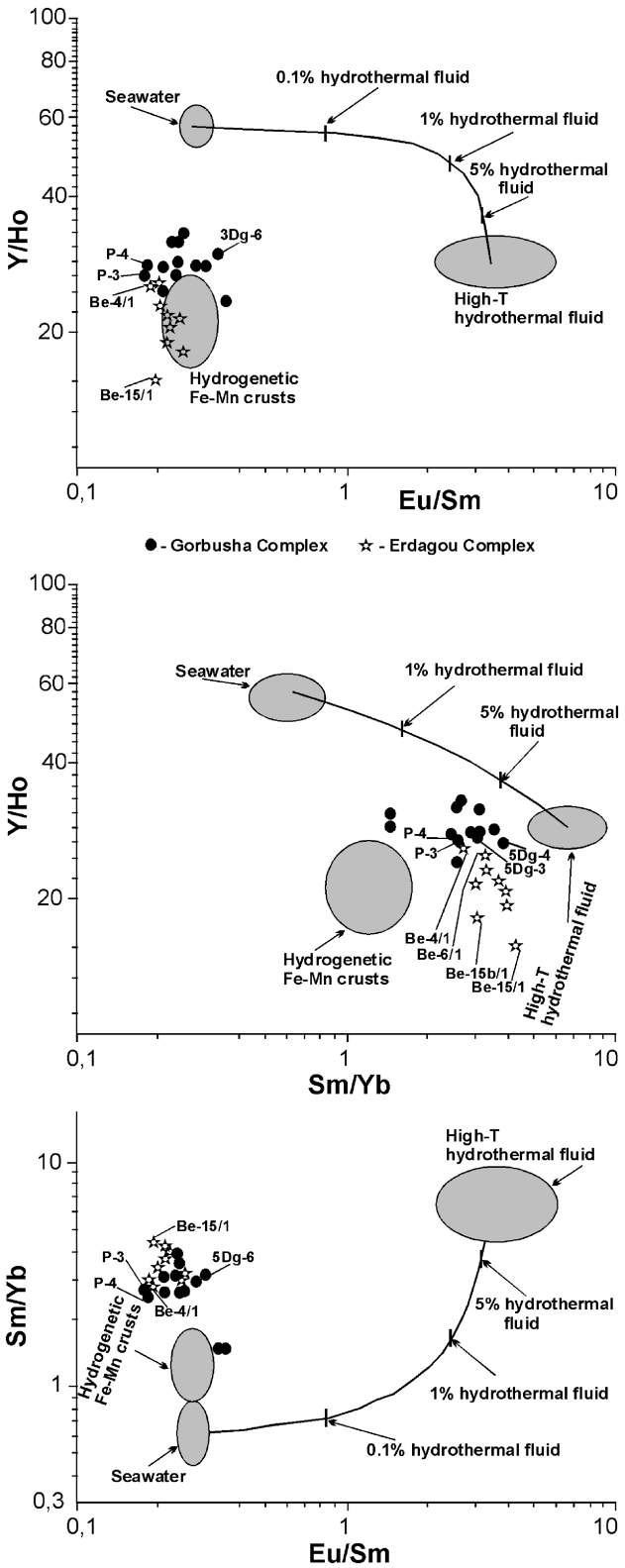

Fig. 7 Diagrams of ratios Y/Ho versus Eu/Sm, Y/Ho versus Sm/Yb and Sm/Yb versus Eu/Sm (according to Alexander et al. 2008) and position on them the figurative points of the Erdagou and Gorbusha Complexes cherty rocks

5 Discussion

The results of the geochemical study of cherty rocks from the different-aged tectono-sedimentary complexes of the Taukha terrane indicate that these rocks were successively and continuously accumulated in the three different depositional environments corresponding at the beginning to the near-spreading ridge area, then open-ocean basin (pelagic area), and, finally, near the continental-margin sedimentation zone. However, even-aged parts of the chert sections of both the above-mentioned complexes were formed at different distances from the spreading ridge. In particular, for the Triassic-Middle Jurassic (up to Callovian) part of the Gorbusha Complex cross-section, a successive change of facies ocean environments is distinguished (see Figs. 5a, c, d, 6d) from the adjacent to the near-spreading zone (in Early Triassic) through pelagic to the peripheral oceanic part bordering the continental-margin depositional area (in Callovian). As for the Erdagou complex, its geological history began only in Late Callovian–Early Oxfordian time. At this time, the Erdagou site of a paleo-oceanic plate was located within the spreading ridge. This is evidenced by the numerous cherts lenses containing late Callovian–Early Oxfordian radiolarians, and hematite deposits (metalliferous sediments) located between the basaltic lava flows, which composed the basement of the Erdagou Complex cross-section (Simanenko et al. 1999). In the Early Kimmeridgian, the Erdagou site of the Paleo-Pacific plate was already located in the near-spreading zone (400 km from the ridge), as evidenced by the geochemical characteristics of the four first meters of cherts overlapping the Erdagou basalts (Kemkin and Kemkina 2015a, b). The Gorbusha site at the same time was moved close to the continental-margin depositional area that evidenced by both the geochemical characteristics of rocks of the Middle Kimmeridgian part of the Gorbusha Complex (see sample R-4 in Figs. 5, 6d), and also by lithological composition of the rocks composing this age level of the Gorbusha cross-section (see Fig. 4). At the Early to Middle Kimmeridgian transition, the dominant chert accumulation was changed to terrigenous sedimentation, i.e., the clayey cherts were gradually replaced by siliceous mudstones.

During the Middle Kimmeridgian–Early Late Tithonian, the Paleo-Pacific plate continued to move towards the Paleo-Asian continent. The Erdagou site of this plate was moved from the near-spreading zone (sample Be-15/1 in Figs. 5, 6d) to the pelagic area (sample Be-12/1 in Figs. 5, 6d), while the Gorbusha site reached the convergent boundary, being moved directly to the near-continental depositional environment (see sample R-3 and R-4 in Figs. 5, 6a, d). Within the Gorbusha complex cross-section, this is also clearly evidenced by changing the

lithological composition of rocks (see Fig. 4), i.e., the siliceous mudstones gradually give way to mudstones and than silty mudstones (sample R-3 was taken 40 cm below the contact of siliceous mudstones and mudstones).

During the Berriasian-Valanginian, the Gorbusha site of the Paleo-Pacific plate subducted and partially accreted to the south-eastern margin of the Paleo-Asian continent. The fragments of its primary sedimentary cover compose nowadays the middle structural level of the Taukha terrane. The Erdagou site at the same time interval, followed to general motion of the Paleo-Pacific plate, continued to change its position relative to the facies oceanic zones and was successively moved from the pelagic depositional environment to the peripheral part of a paleo-ocean immediately adjacent to the continental-margin sedimentation area (see sample Be-10/1, Be-8/1 in Figs. 5a–c, 6d), and then directly to the area of continental-margin depositional environment (sample Be-6/1, Be-4/1 in Figs. 5, 6a, d). Within the Erdagou Complex cross-section, this is also clearly recorded by changing the lithological variety of rocks. In Fig. 3 it can be seen that early Late Tithonian cherts (sample Be-12/1) are replaced upward the section by Late Tithonian–Early Berriasian clayey cherts (samples Be-10/1, Be-8/1) and, further, by Middle-Late Berriasian siliceous mudstones (samples Be-6/1, Be-4/1). At the end of Valanginian-the beginning of the Hauterivian (this is indicated by the age of the siltstones and sandstones part of the Erdagou Complex cross-section), the Erdagou site of the Paleo-Pacific plate reached the convergent boundary and repeated the fate of the Gorbusha site, being subducted and partially accreted to the south-eastern margin of the Paleo-Asian continent.

In the Paleo-Pacific plate drift history, considered on the example of its two sites, there are, as a minimum, two momentous events that allow one to quantify the estimate of the distances of movements of its individual sites and the whole plate as well. These events are the moments (time) of reaching by certain sites of an oceanic plate the area of terrigenous sedimentation (continental-margin depositional zone) and the subduction zone (trench). In the stratigraphic section of the oceanic plate sedimentary cover, these moments are recorded by replacement the pelagic sedimentation by hemipelagic one and then terrigenous. In terms of lithology, this is registered by gradual transition of cherts and clayey cherts into siliceous mudstones, and, further into mudstones, siltstones and sandstones.

According to the data on the distribution and composition of bottom sediments of the World Ocean, summarized by Lisitsyn (1974, 1977, 1978, 1991) in the form of numerous maps of types of bottom sediments, absolute mass schemes, schemes of the distribution of a sedimentary layers by thicknesses, etc., the area of terrigenous sedimentation extends an average of 1000 km from the land-sea border. The exceptions are for the Polar Regions, where it is slightly wider due to the transferring of clastic material by ice and arid zones, where it is a little narrower due to the smaller amount of river runoff. The subduction zone is on average 100–130 km from the coastline (70–75 km is the average shelf width and 55–60 km is the average width of the trenches).

According to radiolarian analysis data (Kemkin and Kemkina 1998, 1999; Kemkin and Taketani 2008), the time of approach to the area of terrigenous sedimentation ($\sim$ 1000 km from the paleocontinent) for the Gorbusha and Erdagou sites of the Paleo-Pacific plate corresponds to the beginning of the Middle Kimmeridgian (155–154 Ma) and the end of Early Berriasian (143–142 Ma), respectively, i.e., the difference is $\sim$ 12 million years. To the subduction zone, the Gorbusha site arrived at the beginning of the Late Tithonian (149–148 Ma), suggesting that the distance of 870–900 km (1000 km − 100–130 km—the width of the shelf plus the trench) was covered in 6 million years. Consequently, the speed of movement of the Paleo-Pacific plate in the period of the beginning of Middle Kimmeridgian-the beginning of Late Tithonian was 14.5–15 cm/year. Correspondingly, the Erdagou site, which approached the area of terrigenous sedimentation 12 million years later, at a drift velocity of 15 cm/year, moved 1800 km. Thus, at the beginning of Middle Kimmeridgian (time of approach of the Gorbusha site to the terrigenous sedimentation area), the Erdagou site was 1800 km distant from it, and from the subduction zone by 2670–2700 km (1800 km + 870–900 km).

During the interval from the beginning of Middle Oxfordian to the beginning of Middle Kimmeridgian, the Erdagou site moved with a speed of 20 cm/year (Kemkin and Kemkina 2015a, b). Consequently, during this 7 Ma period, from 162 to 155 Ma it became closer to the Paleo-Asian continent by another 1400 km. Thus, at the beginning of the Middle Oxfordian, the Erdagou site was 4070–4100 km away from the subduction zone. At this time it represents a part of the spreading ridge, but already not active (basalt effusions were replaced by stable chert accumulation).

At first view, the data obtained are somewhat inconsistent with our previous calculations on the basis of geochemical and lithologic-biostratigraphic studies of chert rocks of the Sikhote-Alin Jurassic accretionary prism,

which indicate that the spreading ridge producing the Paleo-Pacific (Izanagi) plate was distanced from the subduction zone not less than 6500 km (Kemkin et al. 2018). However, disagreements disappear, if we take into account one event that occurred in the ancient Pacific about 175 Ma ago. The event is the birth and subsequent growth of the Pacific plate, which now forms the majority of the bottom of the modern Pacific Ocean. The timing of origin of the Pacific Plate is determined from sets of radiometric and biostratigraphic studies of the core samples of the well 801C ODP (Bartolini and Larson 2001). The reason for the birth of the Pacific plate is considered to be the migration of the triple junction point of the spreading ridges separating the Izanagi (Paleo-Pacific), Farallon, and Phoenix plates (Boschman and van Hinsbergen 2016) and the appearance of a new system of rift zones (see Fig. 8a). As the Pacific plate expanded, the detached fragments of the former system of spreading ridges moved away and drifted in directions perpendicular to the axes of the new rift zones (see Fig. 8b). However, volcanic activity within the detached fragments of the former spreading system periodically took place (probably until the temperature in the magmatic chambers beneath them decreased and magmatic melt was crystallized). For the Erdagou site of the former spreading system, which produced the Paleo-Pacific plate, volcanic activity is recorded up to Early Oxfordian indicated by presence of lenses of Late Callovian–Early Oxfordian cherts between basalt flows, i.e., until the Erdagou site was moved on 2400–2430 km (6500 km − 4070–4100 km) from its original location.

Migration of the Erdagou site together with the detached fragment of the Pre-Middle Jurassic spreading system of Paleo Pacific at the distance of 2400–2430 km took about 11–12 Ma (175 Ma—the Late Toarcian, the birth of the Pacific plate, minus 163–164 Ma—Early Oxfordian, when it was distanced from the subduction zone at 4070–4100 km). Consequently, the speed of motion of the oceanic plate at this time interval was approximately 21–22 cm/year.

In the Jurassic history of the Paleo-Pacific plate drift, there is one important feature, which, in our opinion, has a direct relation to the change of the geodynamic mode on the eastern margin of the Paleo-Asian continent at the Jurassic–Cretaceous transition. During the end of the Late Tithonian, the geodynamic regime of the convergent (subduction) margin along the eastern edge of the Paleo-Asian continent was changed to a setting of transform margin. Only along the part of its southern edge, due to its orthogonal orientation with respect to the direction of motion of an oceanic plate, new Latest Jurassic–Early Cretaceous subduction zone arose (Kemkin 2006; Khanchuk et al. 2016; Kemkin et al. 2016). The analysis of data on the movement speeds of the Paleo-Pacific plate shows

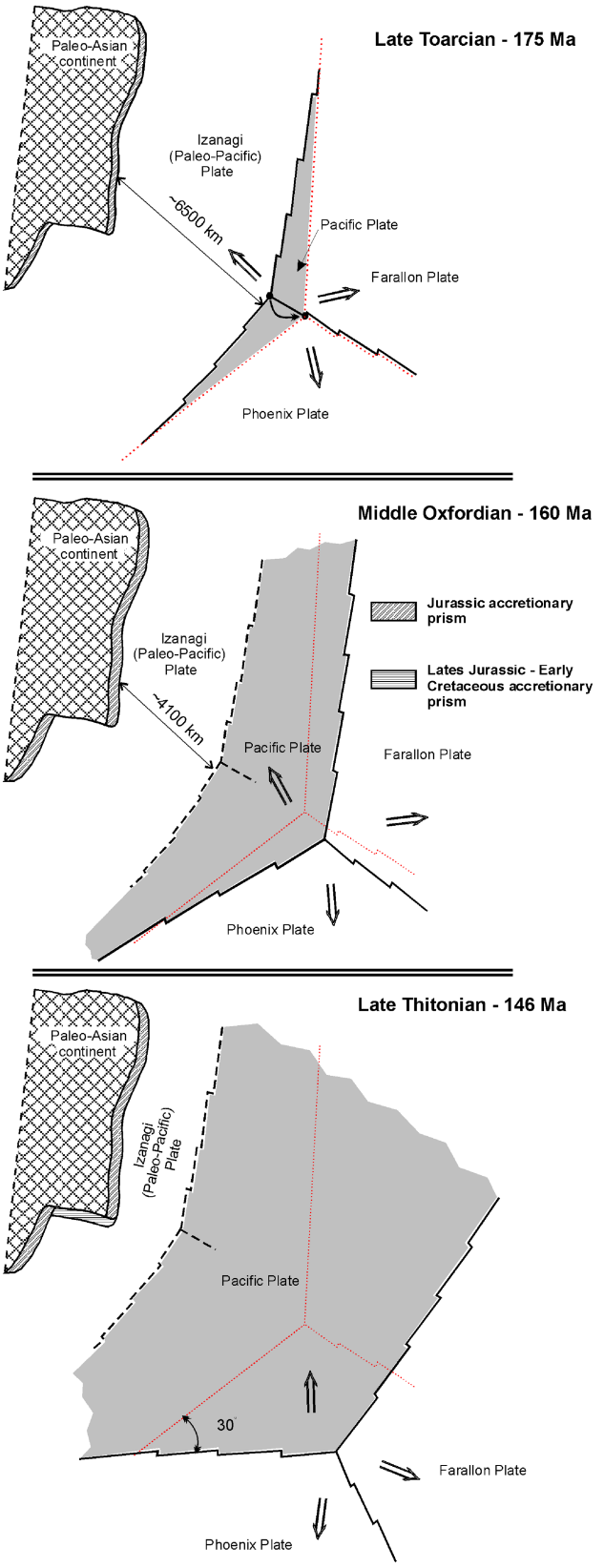

Fig. 8 The emergence of the Pacific rift system and changing its orientation relative to the Paleo-Asian continent in the Middle-Late Jurassic

that its northern part, the fragments of which compose the Jurassic accretionary prism of the Sikhote-Alin orogen, moved with a steadily increasing speed—12–13 cm/year in the Early Jurassic, 14–15 cm/year in the Aalenian-the beginning of Bajocian, 20–21 cm/year in the Bajocian, 21–22 cm/year in the Bathonian-Oxfordian (Kemkin et al. 2016). In contrast, the southern part of the Paleo-Pacific Plate (that is evidenced by the paleobiogeographic data (for example, Tazawa 1993, 2000; Ohana and Kimura 1995; Okada and Sakai 2000; Ehiro 2001; Kimura 2000), the fragments of which compose the Late Jurassic–Early Cretaceous accretion prism of the Sikhote-Alin and Japan, according to calculations given above, moved with gradually decreased speed—21–22 cm/year in the Aalenian–Early Oxfordian, 20 cm/year in the Middle Oxfordian–Early Kimmeridgian, and 15 cm/year in the Middle Kimmeridgian-Late Tithonian. It is obvious that such dynamics of motion of the Paleo-Pacific plate, caused by change in spreading speeds in different parts of the spreading ridge, inevitably had to lead to a changing the relative orientation of the continental margin contour and the axis of the spreading ridge. Direct evidence of this is the southern part of the Atlantic Ocean (see Fig. 9), the gradual opening of which during 139 Ma was reconstructed on the basis of strip magnetic anomalies (e.g., Müller et al. 2008). The Fig. 9 shows that the contour of the South American continent and the axis of the mid-Atlantic ridge, which were parallel to each other at the beginning stage of the opening of the South Atlantic, have changed their mutual orientation to 30° in present coordinates, due to the higher spreading speed in the southern part (this is clearly seen by the width of the magnetic anomalies). Obviously, the magnitude of the rotational angle of the continent contour relative to the spreading ridge axis depends not only on the time but also on the speed of spreading. The opening of the South Atlantic is carried out for almost 139 Ma, and its width at the latitude of Cape Town is about 5500–5700 km. This indicates that the average spreading speed in the southern part of the South Atlantic mid-oceanic ridge was about 4 cm/year. The spreading speed in the Paleo-Pacific was five (sometimes more) times higher than the average opening speed of the South Atlantic. Consequently, the time for turning the continent contour relatively the spreading ridge axis by the same value (30°), at a speed exceeding 5 times, should be 5 times less.

The change of the Paleo-Pacific plate motion speeds, i.e., the decrease for its southern part and the increase for the northern, as shown above, is recorded from the end of the Toarcian (the beginning of the restructuring of the Paleo-Pacific rift system and the birth of the Pacific Plate). This means that the time interval for the turning of the continent contour and the axis of the spreading ridge producing the Pacific plate, which, in turn, moved the Paleo-Pacific plate, is about 28–29 Ma (175 Ma—the formation of a new rift system of Paleo Pacific minus 146–147 Ma—the time of the change of the geodynamic mode on the eastern margin of the Paleo-Asian continent). And this is practically 5 times less (139 Ma divided by 5–27.8 Ma) than the time for opening the South Atlantic.

It is worth mentioning another parameter, namely, the value of the difference of the spreading speed in the different parts of the mid-oceanic ridge, which, obviously, also significantly affects the value of the rotational angle. In the case of the South Atlantic, the difference in the spreading speed in the northern and southern parts of the South Atlantic mid-oceanic ridge was about 1 cm/year. The width of the Atlantic Ocean at the latitude of Salvador is about 4500 km, i.e., the average spreading speed in the

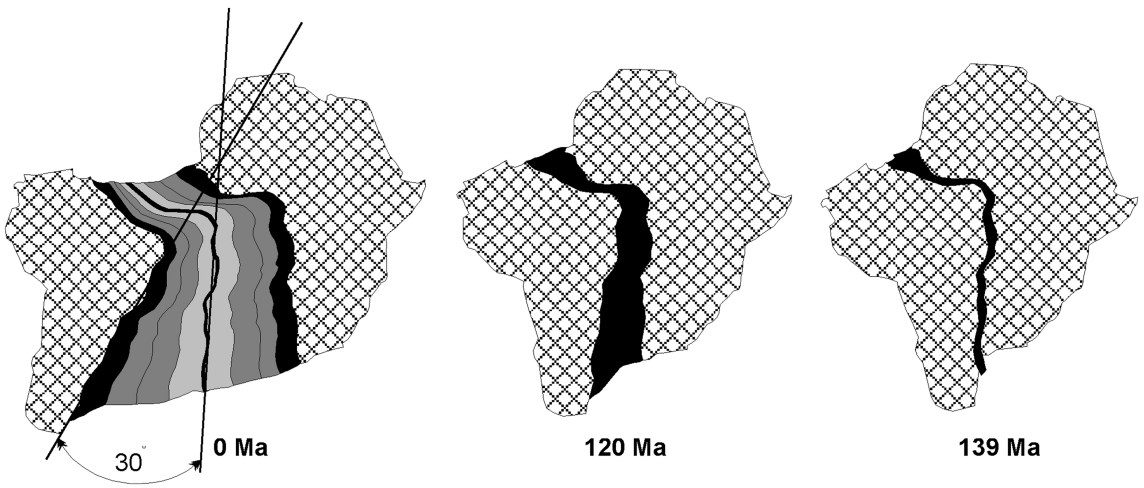

Fig. 9 Reconstruction of the opening of the Atlantic Ocean southern part (based on linear magnetic anomalies)

northern part during 139 Ma was about 3 cm/year, while in the southern part—4 cm/year (see above). For the newly formed Paleo Pacific rift system, the difference in the spreading speed increased steadily from 0 to 7 cm/year, i.e., in average was 3.5 cm/year, starting from the end of Callovian-beginning of Oxfordian (when spreading speed was approximately the same on both northern and southern flanks). Thus, it can be stated with confidence that in the period from Aalenian to the end of Tithonian the Paleo-Asian continent and the spreading ridge determining the direction of motion of the Pacific plate and, correspondingly, the Paleo-Pacific plate, were turned relatively each other not less than 30 degrees and were oriented perpendicularly or near-perpendicularly. This was the reason for the change of the geodynamic mode, since the above-mentioned plates began to move parallel to the Paleo-Asian continent and only along the part of its southern margin, which was oriented orthogonal relatively new direction of the oceanic plates motion (see Fig. 8c), the subduction mode continued.

6 Conclusion

Holistic studies on the composition of cherty rocks from the different-aged tectono-stratigraphic complexes of the Taukha terrain of the Sikhote-Alin Late Jurassic–Early Cretaceous accretionary prism showed that they accumulated within several oceanic facies zones. The formation of stratigraphic cross-sections of each complex started by accumulation of chert sediment at the beginning in the zone adjacent to the spreading ridge, then continued within the abyssal plain, and finished in the peripheral part of a paleo-ocean, directly adjacent to the continental-margin depositional area, where later it was gradually replaced by accumulation of hemipelagic deposits, and then terrigenous ones. These data convincingly evidence the motion of an oceanic floor, within which the cherty sediments accumulated, from the spreading zone to the paleocontinent margin and subsequent successive accretion of fragments of the sedimentary cover different-aged paleo-oceanic plate sites (i.e., different-distanced from the spreading center).

The speeds of the Paleo-Pacific plate motion in the Jurassic are calculated, based upon geochemical data and lithologic-biostratigraphic studies of cherts and siliceous–clayey rocks from different-aged complexes of the Taukha terrain. It shows that during the Toarcian-Latest Tithonian, its northern part moved with a steadily increasing speed (12–13 cm/year in the Early Jurassic, 14–15 cm/year in the Aalenian-beginning of Bajocian, 20–21 cm/year in the Bajocian, and 21–22 cm/year in the Bathonian-Oxfordian), while the motion speed of the Paleo-Pacific plate southern part gradually decreased (22 cm/year in the Bajocian–Early Oxfordian, 20 cm/year in the Middle Oxfordian–Early Kimmeridgian, and 15 cm/year in the Middle Kimmeridgian-Late Tithonian).

Different spreading speeds in the mid-oceanic ridge different parts caused the turn of the Paleo-Asian continent contour relatively the spreading ridge axis by at least 30 degrees that resulted in near orthogonal their orientation. This, in turn, caused a change of direction of the Paleo-Pacific plate motion, which became move parallel to the Paleo-Asian continent eastern margin starting from the end of Tithonian. The changing of interaction style of the paleocontinental and paleooceanic lithospheric plates at the Jurassic–Cretaceous transition predetermined the change in the geodynamic setting on the Paleo-Asian continent eastern edge turning it from convergent margin into transform margin.

Acknowledgements This study was supported in part by Grant of the RFBR-GFEN, Project No. 19-55-53008.

Appendix

See Tables 1, 2, 3, 4 and 5.

Table 1 Composition and contents of major (petrogenic) elements of the Gorbusha Complex cherty rocks

Element (wt%)	Sample												
	R-3	R-4	R-13	R-16a	R-17c	R-20c	R-21f	3Dg-6	3Dg-9a	5Dg-6	5Dg-5	5Dg-4	5Dg-3
SiO_2	82.30	77.90	91.70	85.70	89.75	83.21	90.70	85.80	89.50	90.52	85.64	92.76	89.95
TiO_2	0.29	0.41	0.11	0.19	0.16	0.25	0.06	0.07	0.12	0.06	0.13	0.03	0.07
Al_2O_3	8.70	11.12	3.36	4.35	3.54	5.18	0.96	2.81	3.29	2.15	3.86	1.00	1.66
Fe_2O_3 (total)	2.43	3.34	2.47	5.84	4.00	8.15	7.42	8.85	4.25	6.28	8.54	5.81	7.28
MnO	0.08	0.14	0.23	0.44	0.23	0.62	0.04	0.38	0.26	0.10	0.13	0.10	0.05
MgO	0.99	1.41	0.35	1.06	0.45	0.92	0.10	0.67	0.48	0.30	0.59	0.10	0.32
CaO	1.17	0.71	0.34	0.56	0.43	0.39	0.20	1.05	0.71	0.12	0.17	0.05	0.18
Na_2O	0.24	0.20	0.03	0.01	0.05	0.04	0.05	0.03	0.04	0.02	0.01	0.01	0.04
K_2O	1.95	2.67	0.69	0.35	0.87	0.77	0.26	0.10	0.73	0.39	0.70	0.18	0.43
P_2O_5	0.04	0.06	0.19	0.39	0.21	0.26	0.03	0.70	0.43	0.08	0.11	0.03	0.03
H_2O	Not det.	0.30	Not det.	Not det.	0.42	0.49	0.7	0.50	0.85	0.03	0.13	Not det.	0.03
LOI	2.20	2.10	0.10	1.10	0.23	0.08	Not det.	Not det.	Not det.	0.10	0.13	0.08	0.07
Total	100.38	100.36	99.56	100.00	100.34	100.36	100.51	100.96	100.66	100.13	100.14	100.15	100.11
$Al_2O_3/(Al_2O_3 + Fe_2O_3)$	0.782	0.769	0.576	0.427	0.469	0.389	0.115	0.241	0.436	0.255	0.311	0.147	0.186
Fe_2O_3/TiO_2	8.318	8.221	22.56	30.46	25.69	33.20	125.5	123.6	34.35	113.3	63.99	167.0	102.6
$100*Fe_2O_3/SiO_2$	2.953	4.288	2.694	6.814	4.458	9.794	8.181	10.31	4.751	6.933	9.967	6.263	8.093
$100*Al_2O_3/SiO_2$	10.57	14.27	3.659	5.076	3.940	6.225	1.060	3.280	3.670	2.375	4.503	1.077	1.847
$Fe_2O_3/(100\text{-}SiO_2)$	0.137	0.151	0.298	0.408	0.390	0.485	0.799	0.623	0.405	0.662	0.594	0.802	0.724
$Al_2O_3/(100\text{-}SiO_2)$	0.491	0.503	0.404	0.304	0.345	0.309	0.103	0.198	0.313	0.227	0.269	0.138	0.165
MnO/TiO_2	0.257	0.345	2.067	2.276	1.467	2.544	0.612	5.279	2.120	1.842	1.006	2.873	0.666

not det. not detected

Table 2 Composition and contents of major (petrogenic) and trace elements of the Erdagou Complex cherty rocks

Element	Sample									
	Be-15/1	Be-15b/1	Be-15c/1	Be-14/1	Be-12/1	Be-10/1	Be-8/1	Be-6/1	Be-4/1	PAAS
SiO_2 wt%	76.20	76.27	83.10	82.92	82.40	70.93	69.61	67.09	66.73	62.8
TiO_2	0.32	0.11	0.13	0.24	0.21	0.28	0.62	0.62	0.61	1
Al_2O_3	4.09	3.46	3.32	5.85	5.04	9.90	13.05	14.66	14.90	18.9
Fe_2O_3 (total)	13.41	10.62	9.84	7.13	7.35	6.14	6.03	7.01	6.86	6.5
MnO	1.39	3.21	0.58	0.29	0.19	0.14	0.09	0.12	0.09	0.1
MgO	0.87	1.09	0.45	0.54	0.85	0.97	1.61	2.21	2.05	2.2
CaO	0.41	0.88	0.44	0.32	0.57	0.12	0.20	0.53	0.63	1.3
Na_2O	0.24	0.12	0.59	0.81	0.74	1.10	1.41	1.51	2.02	1.2
K_2O	0.60	0.37	0.73	1.40	1.27	2.53	3.40	3.42	3.04	3.7
P_2O_5	0.07	0.06	0.05	0.07	0.02	0.05	0.07	0.07	0.09	0.2
H_2O	0.60	0.03	0.22	0.10	0.80	0.95	0.80	0.00	0.00	Not def.
LOI	1.70	3.57	0.18	0.90	1.00	6.30	3.60	3.20	3.20	Not def.
Total	99.90	99.78	99.64	100.57	100.43	99.41	100.50	100.42	100.22	Not def.
Li ppm	6.93	21.04	8.71	7.19	6.65	12.07	19.80	34.24	37.33	75
Be	0.70	0.42	0.70	0.66	0.55	0.76	1.78	2.21	2.71	Not def.
Sc	5.8	4.55	3.4	7	4.9	9.9	14.1	13.3	13.7	16
V	112.7	78.6	31.15	38.3	49.15	73.65	93.9	107.4	94.9	150
Cr	81.8	53.1	69.65	54.6	58.35	56.75	66.85	74.4	94.7	110
Co	9.21	21.80	13.88	10.04	6.09	7.71	8.85	14.96	13.22	23
Ni	98.49	168.04	60.39	42.31	32.63	33.30	32.97	46.35	53.39	55
Cu	178.19	73.14	69.74	46.75	29.77	28.32	23.82	35.77	50.34	50
Zn	47.32	103.28	38.02	31.52	26.21	40.15	60.03	84.08	87.63	85
Ga	3.11	5.49	4.62	7.06	3.95	11.32	16.19	19.48	20.04	20
As	4.45	5.81	8.87	11.88	1.80	6.83	6.11	3.82	3.34	Not def.
Rb	11.76	12.81	27.22	40.20	29.14	75.79	109.59	116.59	112.29	160
Sr	41.4	41.65	52.6	56.3	61.95	46.65	60.15	70.85	86.05	200
Y	4.68	6.51	4.51	4.32	2.09	7.98	10.89	11.55	14.88	27
Zr	77.72	5.16	30.88	51.53	43.33	54.97	140.57	149.23	166.88	210
Nb	4.56	1.92	2.35	3.80	3.56	7.73	12.74	12.60	13.36	19
Cd	0.01	0.04	0.04	0.03	0.04	0.03	0.16	0.07	0.06	Not def.
Sn	0.20	2.24	17.06	3.20	2.50	3.10	4.11	3.13	9.15	4
Cs	1.38	1.70	1.42	2.49	2.82	5.16	9.52	10.31	10.81	15
Ba	591	611.5	1057	556	620.8	577	954	659	556.5	650
Hf	2.33	1.16	1.10	1.90	1.74	2.28	5.83	5.70	6.70	5
Ta	0.42	0.20	0.24	0.44	0.29	0.50	1.27	1.36	1.52	Not def.
Tl	0.18	0.18	0.24	0.42	0.22	0.62	0.85	0.62	0.59	Not def.
Pb	22.8	24.62	29.54	3.09	9.77	13.70	16.31	14.68	22.35	20
Th	2.65	2.03	2.21	3.38	2.38	7.96	10.88	9.84	12.19	14.6
U	0.68	0.35	0.58	0.51	0.49	1.40	1.93	1.82	1.87	3.1
$Al_2O_3/(Al_2O_3 + Fe_2O_3)$	0.23	0.25	0.25	0.45	0.40	0.62	0.68	0.67	0.69	
MnO/TiO_2	4.361	2.842	4.536	1.223	0.879	0.471	0.151	0.188	0.148	
Fe_2O_3/TiO_2	42.10	94.11	77.09	29.72	34.86	13.30	9.69	11.28	11.16	
$Fe_2O_3/(100\text{-}SiO_2)$	0.56	0.45	0.58	0.42	0.42	0.21	0.20	0.21	0.21	
$Al_2O_3/(100\text{-}SiO_2)$	0.17	0.15	0.20	0.34	0.29	0.34	0.43	0.45	0.45	
V/Y	24.08	12.07	6.91	8.87	23.52	9.23	8.62	9.30	6.38	
Ti/V	17.02	8.389	25.02	37.57	25.61	22.79	39.58	34.61	38.53	

not def. not defined

Table 3 Composition and contents of trace elements of the Gorbusha complex cherty rocks

Element (ppm)	Sample													
	R-3	R-4	R-13	R-16a	R-17c	R-20c	R-21f	3Dg-6	3Dg-9a	5Dg-6	5Dg-5	5Dg-4	5Dg-3	PAAS
Li	28.15	50.49	14.43	44.70	13.36	39.04	1.81	27.45	14.54	22.13	47.53	14.67	10.55	75
Be	1.35	1.77	0.79	0.55	0.70	0.37	0.18	0.15	0.30	0.34	0.91	0.20	0.27	Not def.
Sc	6.16	8.35	7.62	13.03	7.8	5.6	1.2	10.7	8.5	2.70	4.78	1.50	1.65	16
V	47.59	58.56	48.49	60.71	37.05	38.3	50.75	57.6	20.7	18.87	33.47	18.39	17.91	150
Cr	323.6	186.6	811.4	601.9	26.25	47.5	56.55	68.35	35.05	62.96	79.78	67.61	87.47	110
Co	7.35	5.11	9.53	18.65	6.60	17.91	4.62	9.50	12.41	4.88	6.11	4.34	4.67	23
Ni	20.04	20.09	41.25	55.42	34.77	35.85	35.77	53.24	44.31	28.75	35.61	17.52	22.50	55
Cu	20.09	27.90	31.94	201.7	72.09	46.49	80.49	37.78	71.39	59.64	87.03	65.46	49.82	50
Zn	25.61	72.83	19.03	242.8	17.71	20.80	24.37	58.43	24.23	49.61	136.67	37.98	122.99	85
Ga	9.97	13.33	4.79	7.24	4.85	6.55	1.87	5.38	5.00	3.67	6.06	2.09	2.81	20
As	7.41	1.69	3.33	28.72	15.35	32.25	8.78	50.78	17.21	2.67	47.64	5.29	3.13	Not def.
Rb	95.24	134.74	34.50	17.54	39.58	27.22	11.32	4.32	31.29	16.59	33.13	8.19	17.23	160
Sr	108.3	70.10	48.44	22.18	40.6	40.7	20.15	31.85	44.35	29.22	31.87	13.06	20.60	200
Y	15.76	14.76	18.92	22.50	14.87	15.67	1.48	17.06	26.23	3.43	5.61	1.80	3.39	27
Zr	25.43	31.31	8.01	7.83	26.44	45.88	15.24	16.46	27.73	5.78	8.08	4.69	11.19	210
Nb	6.41	7.21	1.60	2.71	2.49	4.55	1.33	1.26	1.97	1.39	3.11	0.98	1.84	19
Mo	18.21	8.62	49.19	36.29	Not def.	Not def.	Not def.	Not def.	Not def.	1.31	1.55	1.46	2.68	1
Ag	0.09	0.11	0.08	1.27	Not def.	Not def.	Not def.	Not def.	Not def.	0.10	0.45	0.31	0.26	Not def.
Cd	0.05	0.09	0.04	1.21	0.02	0.03	0.26	0.59	0.04	0.07	0.69	0.56	0.21	Not def.
Sn	1.94	1.99	1.21	1.14	10.44	3.03	3.98	4.08	2.58	0.56	1.59	0.52	0.79	4
Sb	Not def.	Not def.	Not def.	Not def.	Not def.	Not def.	Not def.	Not def.	Not def.	1.15	1.55	0.61	1.01	Not def.
Cs	14.62	22.23	9.85	4.44	10.05	6.39	2.80	1.28	8.67	4.44	5.91	1.83	4.93	15
Ba	585.8	544.3	417.9	178.0	465.25	423.7	190.65	99.55	469.75	354.5	226.1	131.8	272.5	650
Hf	0.74	0.89	0.27	0.22	1.13	2.00	0.52	0.56	1.16	0.13	0.19	0.11	0.22	5
Ta	0.39	0.50	0.09	0.17	0.23	0.47	0.10	0.10	0.21	0.10	0.23	0.06	0.12	Not def.
W	13.16	7.40	31.83	24.54	Not def.	Not def.	Not def.	Not def.	Not def.	2.55	3.93	5.19	8.83	2.7
Tl	Not def.	Not def.	Not def.	Not def.	0.42	0.40	0.28	0.05	0.36	0.24	0.40	0.14	0.21	Not def.
Pb	19.04	29.06	6.67	124.1	2.44	7.42	33.27	23	5.76	4.00	31.29	23.50	15.45	20
Th	5.72	6.40	1.61	2.12	2.20	3.50	0.79	1.12	2.30	1.01	2.43	0.65	1.24	14.6
U	1.13	0.92	0.18	0.11	0.32	0.43	0.62	1.36	0.50	0.50	0.33	1.03	1.12	3.1
Ti/V	36.80	41.59	13.54	18.93	25.20	38.42	6.981	7.447	35.85	17.59	23.89	11.34	23.74	
V/Y	3.020	3.968	2.563	2.698	2.491	2.444	34.28	3.377	0.789	5.504	5.968	10.21	5.281	

not def. not defined

Table 4 Contents of REE of the Gorbusha complex cherty rocks

Element (ppm)	Sample												
	R-3	R-4	R-13	R-16a	R-17c	R-20c	R-21f	3Dg-6	3Dg-9a	5Dg-6	5Dg-5	5Dg-4	5Dg-3
La	29.15	25.15	11.53	12.07	12.45	13.96	1.24	7.43	18.32	4.54	7.53	3.46	6.99
Ce	59.94	52.74	27.10	27.38	25.11	27.34	2.54	12.58	31.10	7.16	12.53	5.54	9.37
Pr	6.03	5.40	3.21	3.17	3.05	3.27	0.35	1.72	4.42	0.93	1.86	0.82	1.18
Nd	21.25	19.22	13.57	12.93	12.72	13.53	1.36	7.43	18.78	3.67	6.76	2.42	3.84
Sm	3.86	3.51	3.11	3.01	2.97	3.25	0.30	1.73	4.18	0.80	1.33	0.54	0.85
Eu	0.68	0.63	0.71	0.74	0.70	0.89	0.11	0.57	0.99	0.24	0.28	0.13	0.18
Gd	3.71	3.26	3.49	3.79	3.33	4.18	0.27	2.65	5.08	0.82	1.25	0.53	0.82
Tb	0.52	0.46	0.49	0.58	0.49	0.61	0.05	0.44	0.72	0.12	0.20	0.08	0.12
Dy	2.92	2.73	2.94	3.65	2.78	3.17	0.29	2.87	4.18	0.66	1.17	0.39	0.66
Ho	0.59	0.53	0.60	0.68	0.52	0.56	0.06	0.57	0.82	0.12	0.23	0.07	0.12
Er	1.55	1.45	1.35	1.69	1.30	1.44	0.19	1.54	2.16	0.32	0.62	0.17	0.33
Tm	0.22	0.21	0.19	0.19	0.15	0.17	0.03	0.21	0.26	0.04	0.08	0.02	0.05
Yb	1.46	1.41	0.99	1.13	0.83	1.13	0.21	1.19	1.60	0.26	0.51	0.14	0.27
Lu	0.20	0.20	0.13	0.14	0.11	0.12	0.03	0.16	0.21	0.04	0.07	0.02	0.04
Total	132.09	116.89	69.41	71.14	66.52	73.63	7.03	41.10	92.83	19.71	34.44	14.32	24.81
Ce/Ce*(1)	0.981	0.983	0.968	0.964	0.887	0.881	0.833	0.767	0.752	0.756	0.729	0.717	0.698
Ce/Ce*(2)	0.931	0.920	0.923	0.913	0.889	0.895	0.721	0.820	0.773	0.790	0.644	0.568	0.703
Lu_n/La_n	0.464	0.529	0.731	0.748	0.575	0.584	1.737	1.427	0.755	0.574	0.656	0.411	0.411
Pr_n/Er_n	1.669	1.598	1.023	0.809	1.012	0.977	0.791	0.479	0.883	1.248	1.284	2.048	1.543
Pr_n/Yb_n	1.615	1.503	1.270	1.103	1.438	0.539	0.671	0.566	1.085	1.426	1.429	2.274	1.689
La_n/Ce_n	1.109	1.088	0.970	1.005	1.131	1.165	1.117	1.347	1.343	1.445	1.371	1.426	1.703
La^*_n/Ce^*_n	1.135	1.129	0.989	1.023	1.002	1.010	1.074	0.964	0.984	1.053	1.116	1.226	1.181
Y/Ho	26.846	27.742	31.689	32.916	28.441	27.866	23.205	29.834	31.897	27.862	24.126	26.552	27.678
Eu/Sm	0.175	0.181	0.228	0.247	0.235	0.273	0.352	0.330	0.237	0.296	0.209	0.232	0.207
Sm/Yb	2.635	2.487	3.131	2.664	3.565	2.890	1.454	1.455	2.614	3.113	2.601	3.848	3.086

Table 5 Contents of REE of the Erdagou complex cherty rocks

Element (ppm)	Sample								
	Be-15/1	Be-15b/1	Be-15c/1	Be-14/1	Be-12/1	Be-10/1	Be-8/1	Be-6/1	Be-4/1
La	20.77	11.49	9.09	16.13	11.11	23.86	32.28	22.28	26.54
Ce	16.49	13.95	13.98	22.69	17.48	46.66	71.68	49.78	59.08
Pr	5.10	3.25	2.12	2.55	1.69	5.62	8.41	6.30	7.23
Nd	19.85	13.05	8.38	9.93	6.22	20.66	30.92	23.56	26.48
Sm	3.36	2.57	1.77	1.97	1.17	3.80	5.28	4.39	4.54
Eu	0.65	0.63	0.42	0.43	0.25	0.78	1.12	0.88	0.85
Gd	2.53	2.26	1.65	1.79	1.05	3.42	4.52	3.91	4.08
Tb	0.31	0.34	0.23	0.22	0.13	0.39	0.54	0.47	0.52
Dy	1.61	1.82	1.19	1.11	0.61	2.00	2.74	2.41	2.95
Ho	0.30	0.36	0.21	0.21	0.11	0.35	0.50	0.46	0.58
Er	0.79	0.96	0.59	0.58	0.27	1.09	1.40	1.32	1.67
Tm	0.12	0.14	0.08	0.08	0.04	0.17	0.21	0.19	0.24
Yb	0.78	0.83	0.58	0.50	0.29	1.13	1.41	1.32	1.64

Table 5 continued

Element (ppm)	Sample								
	Be-15/1	Be-15b/1	Be-15c/1	Be-14/1	Be-12/1	Be-10/1	Be-8/1	Be-6/1	Be-4/1
Lu	0.10	0.11	0.07	0.07	0.04	0.15	0.19	0.18	0.22
Total	72.76	51.76	40.36	58.26	40.46	110.08	161.20	117.45	136.62
Ce/Ce* (1)	0.34	0.49	0.69	0.75	0.85	0.87	0.94	0.91	0.92
Ce/Ce* (2)	0.33	0.45	0.68	0.50	1.00	0.80	0.82	0.77	0.79
Lu_n/La_n	0.318	0.613	0.504	0.282	0.240	0.414	0.391	0.547	0.558
Pr_n/Er_n	2.778	1.457	1.546	1.892	2.694	2.219	2.585	2.054	1.863
Pr_n/Yb_n	2.566	1.537	1.434	2.001	2.287	1.952	2.341	1.873	1.730
La_n/Ce_n	2.87	1.88	1.48	1.62	1.45	1.17	1.03	1.02	1.02
La^*_n/Ce^*_n	1.064	1.037	1.051	0.588	1.106	1.107	1.107	1.095	1.110
Y/Ho	15.600	18.083	21.476	20.571	19.000	22.800	21.780	25.109	25.655
Eu/Sm	0.193	0.245	0.237	0.218	0.214	0.205	0.212	0.200	0.187
Sm/Yb	4.308	3.096	3.052	3.940	4.034	3.363	3.745	3.326	2.768

References

Alexander BW, Bau M, Andersson P, Dulski P (2008) Continentally-derived solutes in shallow Archean sea water: rare earth element and Nd isotope evidence in iron formation from the 2.9 Ga Pongola Supergroup, South Africa. Geochim Cosmochim Acta 72(2):378–394

Barcelo D (ed) (2003) Comprehensive analytical chemistry, vol XLI. Elsevier, Amsterdam

Bartolini A, Larson RL (2001) Pacific microplate and the Pangea supercontinent in the early to middle Jurassic. Geology 29(8):735–738

Bau M, Dulski P (1996) Distribution of Y and rare-earth elements in the Penge and Kuruman iron formations, Transvaal Supergroup, South Africa. Precambrian Res 79:37–55

Berger WH, Winterer EL (1974) Plate stratigraphy and fluctuating carbonate line. In: Hsu KJ, Jehkyns H (eds) Pelagic sediments on land and under the sea. Wiley, Berlin, pp 11–48

Bonatti E, Fisher DE, Joensuu O, Rydell HS (1971) Postdepositional mobility of some transition elements, phosphorous, uranium and thorium in deep sea sediments. Geochim Cosmochim Acta 35:189–201

Boschman LM, van Hinsbergen DJJ (2016) On the enigmatic birth of the Pacific Plate within the Panthalassa Ocean. Sci Adv 2(7):1–6

Brueckner HK, Snyder WS (1985) Chemical and Sr isotopic variations during diagenesis of Miocene siliceous sediments of the Monterey Formation, California. J Sediment Res A 55:553–568

Brueckner HK, Snyder WS, Boudreau M (1987) Diagenetic controls on the structural evolution of siliceous sediments in the Golconda Allochthon, Nevada, USA. J Struct Geol 9:403–417

Buslov MM (2011) Tectonics and geodynamics of the Central Asian fold belt: the role of the Late Paleozoic large-amplitude strike-slips. Russ Geol Geophys+ 52(1):66–90 **(in Russian)**

Chen D, Qing H, Yan X, Li H (2006) Hydrothermal venting and basin evolution (Devonian, South China): constraints from rare earth element geochemistry of chert. Sediment Geol 183(3/4):203–216

Courtois C, Hoffert M (1977) Distribution des terres rares dans les sediments superficiels du Pacifique sudest. Bull Soc Geol Fr 7:1245–1251

Du Y, Zhu J, Gu S (2007) Sedimentary geochemistry of chert from the Middle-Upper Ordovician in Shihuigou area, North Qilian orogenic belt and its tectonic implication. Front Earth Sci 1(1):30–36

Dubinin AV (1994) Geochemistry of rare-earth elements in sediments and nodules of the Guatemalan Hollow of the Pacific Ocean: the influence of the processes of early diagenesis. Geochem Int 8–9:1335–1345 **(in Russian)**

Dubinin AV (1998) Rare-earth elements in the processes of early diagenesis of Pacific ocean sediments. Lithol Miner Resour+ 4:346–354 **(in Russian)**

Dubinin AV (2006) Geochemistry of rare-earth elements in the ocean. Nauka, Moscow **(in Russian)**

Ehiro M (2001) Origin and drift histories of some microcontinents distributed in the eastern mardin of Asian continent. Earth Sci 55(2):71–81

Elderfield H, Greaves MJ (1982) The rare earth elements in seawater. Nature 296:214–219

Engebretson DC, Cox A, Gordon RG (1985) Relative motion between oceanic and continental plates in the Pacific basin. Bull Geol Soc Am 206:1–59

German CR, Klinkhammer GP, Edmond JM, Mitra A, Elderfield H (1990) Hydrothermal scavenging of rare-earth elements in the ocean. Nature 345:516–518

Gromet LP, Dymek RF, Haskin LA, Korotev RL (1984) The "North American Shale Composite", its compilation, major and trace element characteristics. Geochim Cosmochim Acta 48:2469–2482

Halamič J, Marchig V, Goričan Ŝ (2001) Geochemistry of triassic radiolarian cherts in North-Western Croatia. Geol Carpath 52(6):327–342

Hein JR, Koski RA (1987) Bacterially mediated diagenetic origin for chert-hosted manganese deposits in the Franciscan Complex, California Coast Ranges. Geology 15:722–726

Isozaki Y, Maruyama S, Furuoka F (1990) Accreted oceanic materials in Japan. Tectonophysics 181(1–2):179–205

Kang J, Zhang Z, Zhang D, Huang H, Dong S, Zhang S (2011) Geochronology and Geochemistry of the Radiolarian Cherts of the Mada'er Area, Southwestern Tianshan: implications for Depositional Environment. Acta Geol Sin Engl 85(4):801–813

Kato Y, Ohta I, Tsunematsu T, Watanabe Y, Isozaki Y, Maruyama S, Imai N (1998) Rare earth element variations in mid-Archean banded iron formations: implications for the chemistry of ocean and continent and plate tectonics. Geochim Cosmochim Acta 62(21–22):3475–3497

Kato Y, Nakao K, Isozaki Y (2002) Geochemistry of Late Permian to Early Triassic pelagic cherts from southwest Japan: implications for an oceanic redox change. Chem Geol 182:15–34

Kemkin IV (2006) Geodynamic evolution of the Sikhote-Alin and the Sea of Japan region in the Mesozoic. Nauka, Moscow **(in Russian)**

Kemkin IV, Kemkina RA (1998) Jurassic–Early cretaceous biostratigraphy of cherty and terrigenous deposits of the Dalnegorsk Ore Region (South Sikhote-Alin). Russ J Pac Geol 17(1):59–76 **(in Russian)**

Kemkin IV, Kemkina RA (1999) Radiolarian biostratigraphy of the Jurassic–Early Cretaceous chert-clastic sequence in the Taukha Terrane (South Sikhote-Alin, Russia). Geodiversitas 21(4):675–685

Kemkin IV, Kemkina RA (2000) Taukha terrane of the southern Sikhote-Alin: structure and formation conditions. Geotectonics+ 5:71–79 **(in Russian)**

Kemkin IV, Kemkina RA (2015a) Geochemical evidence of oceanic origin of cherts of accretionary complexes of Sikhote-Alin. Geochem Int 8:706–719 **(in Russian)**

Kemkin IV, Kemkina RA (2015b) Depositional environment of cherts of the Sikhote-Alin region (Russia Far East): evidence from major, trace and Rare Earth Elements geochemistry. J Earth Sci China 26(2):259–272

Kemkin IV, Taketani Y (2008) Structure and age of lower structural unit of the Taukha terrane of Late Jurassic–Early Cretaceous accretionary prism, Southern Sikhote-Alin. Isl Arc 17(4):517–530

Kemkin IV, Khanchuk AI, Kemkina RA (2016) Accretionary prisms of the Sikhote-Alin orogenic belt: composition, structure and significance for reconstruction of the geodynamic evolution of the eastern Asian margin. J Geodyn 102:202–230

Kemkin IV, Khanchuk AI, Kemkina RA (2018) Geochemical features of the cherts of the Samarka terrane (Sikhote-Alin) and the scale of the accreted paleo-oceanic plate. Russ Geol Geophys+ 59(2):143–157 **(in Russian)**

Khanchuk AI (2000) Paleogeodynamic analysis of the formation of ore deposits of the Far East of Russia. In: Khanchuk AI (ed) Ore deposits of continental margins. Dal'nauka, Vladivostok, pp 5–34 **(in Russian)**

Khanchuk AI (ed) (2006) Geodynamics, Magmatism and Metallogeny of the Russian east. Book 1. Dal'nauka, Vladivostok, p 572 **(in Russian)**

Khanchuk AI, Kemkin IV, Kruk NN (2016) The Sikhote-Alin orogenic belt, Russian South East: terranes and the formation of continental lithosphere based on geological and isotopic data. J Asian Earth Sci 120:117–138

Kimura T (2000) Early Cretaceous climatic provinces in Japan and adjacent regions on the basis of fossil land plants. In: Okada H, Mateer NJ (eds) Cretaceous environments of Asia. Elsevier, Amsterdam, pp 155–161

Kröner A (ed) (2015) The Central Asian Orogenic Belt: geology, evolution, tectonics and models. Borntaeger Science Publisher, Stuttgart

Kunimaru T, Shimizu H, Takahashi K, Yabuki S (1998) Differences in geochemical features between Permian and Triassic cherts from the Southern Chichibu terrane, southwest Japan: REE abundances, major element compositions and Sr isotopic ratios. Sediment Geol 119:195–217

Lawrence MG, Kamber BS (2006) The behaviour of the rare earth elements during estuarine mixing—revisited. Mar Chem 100:147–161

Lawrence MG, Greig A, Collerson KD, Kamber BS (2006) Rare earth element and yttrium variability in South East Queensland Waterways. Aquat Geochem 12:39–72

Li X (2000) Geochemistry of the Late Paleozoic radiolarian cherts within the NE Jiangxi ophiolite melange and its tectonic significance. Sci China Ser D 43(6):617–624

Lisitsyn AP (1974) Sediment formation in the oceans. Nauka, Moscow **(in Russian)**

Lisitsyn AP (1977) Terrigenous sedimentation, climatic zonality and interaction of terrigenous and biogenic material in the oceans. Lithol Miner Resour+ 6:3–22 **(in Russian)**

Lisitsyn AP (1978) Ocean sedimentation processes. Nauka, Moscow **(in Russian)**

Lisitsyn AP (1991) Terrigenous sedimentation processes in the seas and oceans. Nauka, Moscow **(in Russian)**

Müller RD, Sdrolias M, Gaina C, Roest WR (2008) Age, spreading rates and spreading symmetry of the world's ocean crust. Geochem Geophy Geosy 9:Q04006. https://doi.org/10.1029/2007gc001743

Murray RW (1994) Chemical criteria to identify the depositional environment of chert: general principles and applications. Sediment Geol 90:213–232

Murray RW, Buchholtz ten Brink MR, Jones DL, Gerlach DC, Ruth GP III (1990) Rare earths elements as indicator of different marine depositional environments in chert and shale. Geology 18:268–272

Murray RW, Buchholtz ten Brink MR, Gerlach DC, Ruth GP III, Jones DL (1991) Rare earth, major, and trace elements in chert from the Franciscan Complex and Monterey Group, California: assessing REE sources to fine-grained marine sediments. Geochim Cosmochim Acta 55:1875–1895

Ohana T, Kimura T (1995) Late Mesozoic phytogeography in Eastern Eurasia, with special reference to the origin of angiosperms in time and site. In: Proceedings of 15th international symposium of Kyungpook National University, pp 293–328

Okada H, Sakai T (2000) The Cretaceous system of the Japanese Islands and its physical environments. In: Okada H, Mateer NJ (eds) Cretaceous environments of Asia. Elsevier, Amsterdam, pp 113–144

Parfenov LM, Kuzmin MI (eds) (2001) Tectonics, geodynamics and metallogeny of the territory of the Republic of Sakha (Yakutia). Nauka-Interperiodica, Moscow **(in Russian)**

Parfenov LM, Berzin NA, Khanchuk AI et al (2003) Model of the formation of orogenic belts in central and northeast Asia. Russ J Pac Geol 22(6):7–41 **(in Russian)**

Piper DZ, Graef PA (1974) Gold and rare-earth elements in sediments from the East Pacific Rise. Mar Geol 17:287–297

Ruhlin DE, Owen RM (1986) The rare-earth element geochemistry of hydrothermal sediments from the East Pacific Rise: examination of a seawater scavenging mechanism. Geochim Cosmochim Acta 50:393–400

Shimizu H, Masuda A (1977) Cerium in chert as an indication of marine environment of its formation. Nature 266:346–348

Sholkovitz ER, Landing WM, Lewis BL (1994) Ocean particle chemistry: the fractionation of rare earth elements between suspended particles and seawater. Geochim Cosmochim Acta 58:1567–1579

Sholkovitze ER (1990) Rare earth elements in marine sediments and geochemical standards. Chem Geol 88:333–347

Simanenko VP, Golozubov VV, Kemkin IV (1999) Basalts of the Erdagou Formation of Primorye and the geodynamic conditions of their formation. Russ J Pac Geol 18(5):82–89 **(in Russian)**

Strekopytov SV, Dubinin AV, Volkov II (1999) General patterns of behavior of rare-earth elements in the pelagic sediments of the Pacific Ocean. Lithol Miner Resour+ 2:133–145 **(in Russian)**

Sugisaki R, Yamamoto K, Adachi M (1982) Triassic bedded cherts in central Japan are not pelagic. Nature 298:644–647

Taylor SR, McLennan SM (1985) The continental crust: its composition and evolution. Blackwell, Oxford

Tazawa J (1993) Pre-Neogene tectonics of the Japanese Islands from the viewpoint of paleobiogeography. J Geol Soc Jpn 99(7):525–543

Tazawa J (2000) Permian brachiopod faunas and pre-Neogene tectonics in the Inner Side of Southwest Japan. Monograph (Chidanken Senpo) 49:5–22

Thassanapak H, Udchachon M, Chonglakmani C (2011) Geochemistry of middle Triassic radiolarian cherts from Northern Thailand: implication for depositional environment. J Earth Sci 22(6):688–703

Toyoda K, Nakamura Y, Masuda A (1990) Rare earth elements of Pacific pelagic sediments. Geochim Cosmochim Acta+ 54:1093–1103

Yamamoto K (1987) Geochemical characteristics and depositional environments of cherts and associated rocks in the Franciscan and Shimanto Terranes. Sediment Geol 52:65–108

Zhang C, Zhou D, Lu G, Wang J, Wang R (2006) Geochemical characteristic and sedimentary environments of cherts from Kumishi ophiolitic mélange in Southern Tianshan. Acta Petrol Sin 22(1):57–64 **(in Chinese with English abstract)**